Chemical ecology of a tripartite symbiosis

Nicholas C. Mucci[1], *Katarina A. Jones*[2], *Mengyi Cao*[3], *Michael R. Wyatt II*[4], *Shane Foye*[5], *Sarah Kauffman*[1], *Michela Taufer*[4], *Yoshito Chikaraishi*[6], *Shawn Steffan*[5, 7], *Shawn Campagna*[2,8], *Heidi Goodrich-Blair*[1,3#]

[1]Department of Microbiology, University of Tennessee-Knoxville, Knoxville TN, USA

[2]Department of Chemistry, University of Tennessee-Knoxville, Knoxville TN, USA

[3]Department of Bacteriology, University of Wisconsin-Madison, Madison WI, USA

[4]Department of Electrical Engineering and Computer Science, University of Tennessee-Knoxville, Knoxville TN, USA

[5]Department of Entomology, University of Wisconsin-Madison, Madison WI, USA

[6]Department of Biogeochemistry, Japan Agency for Marine-Earth Science and Technology, Yokosuka 237-0061, Japan

[7]US Department of Agriculture, Agricultural Research Service, Madison WI, USA

[8]Biological and Small Molecule Mass Spectrometry Core, University of Tennessee-Knoxville, Knoxville TN, USA

#Corresponding author: Heidi Goodrich-Blair, hgblair@utk.edu

ABSTRACT

Microbial symbiotic interactions, mediated in part by small molecule signaling, drive physiological processes of higher order systems, including the acquisition and consumption of nutrients that support symbiotic partner reproduction. Advances in metabolic analytic technologies provide new avenues to examine how chemical ecology, or the conversion of existing biomass to new forms, changes over a symbiotic lifecycle. Here we examine such processes using the tripartite relationship involving the nematode host *Steinernema carpocapsae*, its obligate mutualist bacterium, *Xenorhabdus nematophila*, and the insects they infect together. The nematode infective juveniles infect insects into which they release bacteria that help suppress insect immunity and kill the insect. The nematode-bacterium pair consume the insect cadaver and reproduce until nutrients are depleted, causing a new generation of infective juvenile nematodes, colonized by the bacterial symbiont, to leave the cadaver in search of insect prey. To begin to understand the processes by which insect biomass is converted over time to either nematode or bacterium biomass, we took a three-pronged approach integrating information from trophic, metabolomics, and gene regulation analyses. Trophic analysis established bacteria as the primary insect consumers, with nematodes at a trophic position of 4.37, indicating consumption of bacteria and likely also other nematodes. Metabolic changes associated with bioconversion of *Galleria mellonella* insects were assessed using multivariate statistical analyses of metabolomics datasets derived from sampling over an infection time course. Statistically significant, discrete phases were distinguishable from each other, indicating the insect chemical environment changes reproducibly during bioconversion. Tricarboxylic acid (TCA) cycle components and amino acids such as proline and leucine were significantly affected throughout the infection. Hierarchical clustering revealed a similar molecular abundance fluctuation pattern for nucleic acid, amino acid, and lipid biosynthesis metabolites. Together, these findings contribute to an ongoing understanding of how symbiont associations shape chemical environments.

IMPORTANCE

The biological world depends on microbial processes, including symbiotic exchanges among mutualists and antagonists. Technical advances have enabled investigation of microbial trophic positions within communities and the identification of metabolites exchanged between microbes and their hosts. These tools were applied to the tripartite *Xenorhabdus* bacteria-*Steinernema* nematode-*Galleria* insect symbiosis. Trophic analyses demonstrate the primary consumer of the insect are the bacteria, and in turn the nematode consumes the bacteria. This suggests the *Steinernema-Xenorhabdus* mutualism is a form of agriculture in which the nematode cultivates their bacterial food source by inoculating them into insect hosts. Metabolomics analysis revealed a shift in biological material throughout progression of the lifecycle: active infection, insect death, and conversion of cadaver tissues into bacterial biomass and nematode tissue. We show that each phase of the lifecycle is metabolically distinct, with significant differences in tricarboxylic acid cycle and amino acid metabolism. Our findings demonstrate that symbiotic lifecycles can be defined by reproducible stage-specific chemical signatures, enhancing our broad understanding of metabolic processes that underpin a three-way symbiosis.

INTRODUCTION

Symbiotic interactions are ubiquitous in biological systems and have shaped the evolution of life {Margulis, 1981}. These long-term, intimate associations are driven by small molecule signaling between partners. Bacterial populations establish diverse and expansive metabolite-mediated signaling networks that control gene expression and downstream behaviors, such as biofilm formation and the production of host-interacting effectors {Camilli, 2006; Worthington, 2012; Chaston, 2012}. A common mechanism by which bacteria sense and transduce metabolic signals is through transcription factors whose DNA binding affinity or specificity is modulated by binding metabolite ligands. For instance, LysR-type transcription factors, which are conserved across proteobacteria, are characterized by a conserved *N*-terminal DNA-binding domain and a *C*-terminal domain that varies among LysR-type regulator homologs. The latter domain is responsible for ligand metabolite binding and dictates the response specificity of the transcription factor {Budnick, 2020; Henikoff, 1988; Maddocks, 2008}. In a range of bacteria, LysR-type regulators modulate various phenotypes, including virulence, nutrient uptake and metabolic homeostasis, motility, quorum sensing, and antibiotic resistance {Abdelhamed, 2020}. Another diverse family of transcription factors, feast/famine regulatory factors like leucine-responsive regulatory protein (Lrp), will bind and dimerize with amino acids in response to nutrient levels and globally induce transcriptional changes {Yokoyama, 2006}.

Given the key function of metabolites in communicating information about intracellular and extracellular environmental conditions, examining their identities and abundances is critical to understanding biological systems. Metabolomics has enabled such studies and has been used to detect specific small molecules that drive essential cellular processes and inter-kingdom signaling {Tang, 2011; Clarke, 2008; Phelan, 2014}. Further, it is being applied to more complex ecosystems comprising multi-species microbiota colonizing a host {Dong, 2019}. However, to date such studies have been primarily focused on binary conditional comparisons between

treatments, or on single, snapshot sampling of complex interactions. Here, to gain insights temporal changes in metabolic pathways that occur in complex ecosystems, a longitudinal analysis of metabolic profiles was conducted in closed ecosystem in which biomass is being reproducibly converted from one type of living organism to another. The closed ecosystem comprised an individual insect infected with an entomopathogenic nematode (EPN) and bacterium (EPNB) pair.

EPNs of the genera *Steinernema* and *Heterorhabditis* associate with mutualistic bacteria in the genera *Xenorhabdus* and *Photorhabdus,* respectively. An infective juvenile (IJ) stage of EPN carry their mutualistic bacteria in their intestine as they dwell in the soil seeking insect hosts to infect. Upon infection, the bacteria are released into the insect blood cavity and together the nematode and bacterium kill and consume the insect for their own reproduction before developing into the bacteria-colonized infective stage again to repeat the cycle {Richards, 2009; Stock, 2019}. EPNBs have been applied as insecticide alternatives to promote agricultural productivity and to help prevent transmission of insect diseases like dengue and West Nile virus {Lacey, 2012; Javal, 2019; da Silva, 2020}.

In this study, consumption and bioconversion of the insect *Galleria mellonella* by the EPN *Steinernema carpocapsae* and its mutualistic bacterial symbiont, *Xenorhabdus nematophila* was examined from a metabolic perspective. *G. mellonella* is used for laboratory isolation and propagation of EPNB, is a model host to understand virulence of a variety of microbial pathogens {Tsai, 2016; Ramarao, 2012} and has a characterized metabolome {Killiny, 2018}. The *S. carpocapsae-X. nematophila* pair was chosen due to the wealth of information available about them from molecular, cellular, and genetic studies {Martens, 2004; Stock, 2019}. For example, it is known that *X. nematophila* bacterial effectors and natural products suppress insect immunity, kill insect blood cells, degrade insect tissues, and defend the insect cadaver from opportunistic competitors {Herbert, 2007}. Also, *X. nematophila* bacteria are essential for *S. carpocapsae* reproduction; in the absence of bacteria fewer nematode IJs emerge from

insect cadavers after reproduction {Mitani, 2004}. Expression of effectors and physiological adaptation to changing host environments is controlled in *X. nematophila* by transcriptional regulators that are predicted to sense and respond to prevailing metabolic conditions {Richards, 2008}. For instance, the LysR-type regulator LrhA that is necessary for *X. nematophila* virulence and controls expression of an extracellular phospholipase that is necessary for insect degradation {Richards, 2008; Richards, 2009; Richards, 2010}, the sigma factor RpoS that is necessary for colonizing the IJ stage of the nematode {Vivas, 2001}, the two-component system CpxRA, and the leucine-responsive regulatory protein Lrp, both of which are necessary for normal virulence and mutualism behaviors {Herbert, 2007; Herbert-Tran, 2009a; Herbert-Tran, 2009b, Cowles, 2007; Herbert, 2007}, NilR, a lambda like repressor family transcription factor that negatively regulates genes necessary for nematode colonization {Cowles, 2006} and the two-component system OmpR/EnvZ that negatively controls *X. nematophila* swarming motility behavior and exoenzyme production {Park and Forst, 2006}. Further, *X. nematophila* displays phenotypic heterogeneity with respect to behaviors important for adaptation to host environments. For instance, “primary form” [1°] *X. nematophila* can be distinguished from “secondary form” [2°] by its motility, antibiotic and natural products secretion, and hemolytic and lipolytic activities and additional phenotypic variants arise over the course of insect infection {Volgyi, 1989; Givaudan, 1995; Cambon, 2019}.

The goal of this study was to begin to understand the overall metabolic transformations, or bioconversion processes occurring within a closed yet complex biological ecosystem. ^{15}N isotopic enrichment analyses were performed to establish the relative trophic positions of the insect, *G. mellonella*, the nematode, *S. carpocapsae*, and the bacterium, *X. nematophila*, so that the relative roles in bioconversion of each ecosystem member could be established. Then, a metabolomics analysis using an ultra-high performance liquid chromatography high-resolution mass spectrometry (UHPLC-HRMS) metabolomics technique was conducted over a 16-day

time course after *S. carpocapsae-X. nematophila* infection of *G. mellonella*, encompassing a complete bioconversion of insect tissues to the bacterial-colonized progeny IJs that emerged from the insect.

RESULTS

Trophic analysis reveals *S. carpocapsae* nematodes directly feed on *X. nematophila* bacteria *in vitro* and *in vivo*:

In vitro trials

The trophic identities of the entomopathogenic nematode (*Steinernema carpocapsae*), its bacterial symbiont (*Xenorhabdus nematophila*), and their host insect were measured empirically based on ^{15}N isotopic enrichment of amino acids (Table 1 and File S1). To this end, it was first necessary to establish that the degree of ^{15}N-enrichment between the consumers (nematodes, bacteria) and their respective diets (e.g., agar growth media, bacteria, or the insect) was consistent with past studies of inter-trophic enrichment (Chikaraishi, 2009; Chikaraishi, 2011; Steffan 2013; Steffan, 2015). This past work relied upon compound-specific isotopic analyses of select amino acid pools, particularly the degree of ^{15}N-enrichment between two amino acids—glutamic acid (glu) and phenylalanine (phe). The differential enrichment between these two amino acids provides a measure of inter-trophic enrichment, which is largely attributable to an organism's assimilation of dietary amino acids (Chikaraishi, 2007; Chikaraishi, 2009; Takizawa, 2020). Such inter-trophic enrichment has been referred to as the trophic discrimination factor ($TDF_{glu\text{-}phe}$), and in carefully controlled feeding studies among diverse consumer groups in the Animalia, Fungi, and Bacteria, the $TDF_{glu\text{-}phe}$ has averaged approximately 7.2‰ (Steffan, 2015; Steffan, 2017). Here, following controlled-feeding *in vitro* trials, the nematodes and bacteria were shown to have both registered $TDF_{glu\text{-}phe}$ values in line with past findings (Fig. 2A). Specifically, the mean (± SE) $TDF_{glu\text{-}phe}$ value exhibited by nematodes cultured on bacterial lawns was 7.41 ± 0.22‰ (N = 14). When parsed by nematode stage, the $TDF_{glu\text{-}phe}$ values of adult and infective juvenile nematodes were, respectively, 6.96 ± 0.16‰ (N = 8) and 8.02 ±

0.36‰ (N = 6). Nematodes fed exclusively a diet of homogenized insect biomass produced a TDF of 7.38 ± 0.05‰ (N = 3). Collectively, the nematode TDF was 7.40 ± 0.18‰ (N = 17). The bacterial symbiont, *Xenorhabdus*, which had been cultured on agar growth media, registered a $TDF_{glu\text{-}phe}$ of 6.53 ± 0.20‰ (N = 6). The mean $TDF_{glu\text{-}phe}$ across both the nematodes and bacteria in this food-chain was 7.18 ± 0.16‰, which did not represent a significant departure from the generalized 7.2‰ $TDF_{glu\text{-}phe}$ benchmark (t_{22} = -0.14, P = 0.893). Given the degree of inter-trophic enrichment exhibited in the nematodes and bacteria, these consumer groups were consistent with the enrichment patterns of heterotrophs across terrestrial, marine, and freshwater systems, allowing for trophic position estimation using established isotopic protocols (Chikaraishi, 2007; Chikaraishi, 2009; Chikaraishi, 2011; Steffan, 2013; Steffan, 2015; Steffan, 2017; Takizawa, 2020).

Using compound-specific isotopic analysis of amino acids, the trophic identities of consumers and their respective diets within the *in vitro* food-chain were measured. At the base of the food-chain, the agar growth media registered a trophic position ($TP_{glu\text{-}phe}$) of 1.0 ± 0.04‰ (N = 3), and the bacteria feeding upon the agar registered at 1.9 ± 0.03‰ (N = 6), which represented approximately one trophic level higher than their diet. Correspondingly, the adult and infective juvenile nematodes that had fed upon the bacteria registered, respectively, at 2.90 ± 0.02‰ (N = 8) and 3.0 ± 0.06‰ (N = 6), which, as predicted, was exactly one trophic level higher than their diet. The homogenate of insect biomass was measured at 2.2 ± 0.02‰ (N = 6), and the nematodes feeding exclusively on this homogenate registered at 3.2 ± 0.01‰ (N = 4), which again demonstrated that when the nematodes consumed a given diet, they registered one trophic level higher. The *in vitro* food-chain effectively compartmentalized each consumer group and thereby provided a means to confirm that when the nematodes or bacteria consumed a given diet, their isotopic compositions enriched consistently and produced predictable trophic position estimates.

189

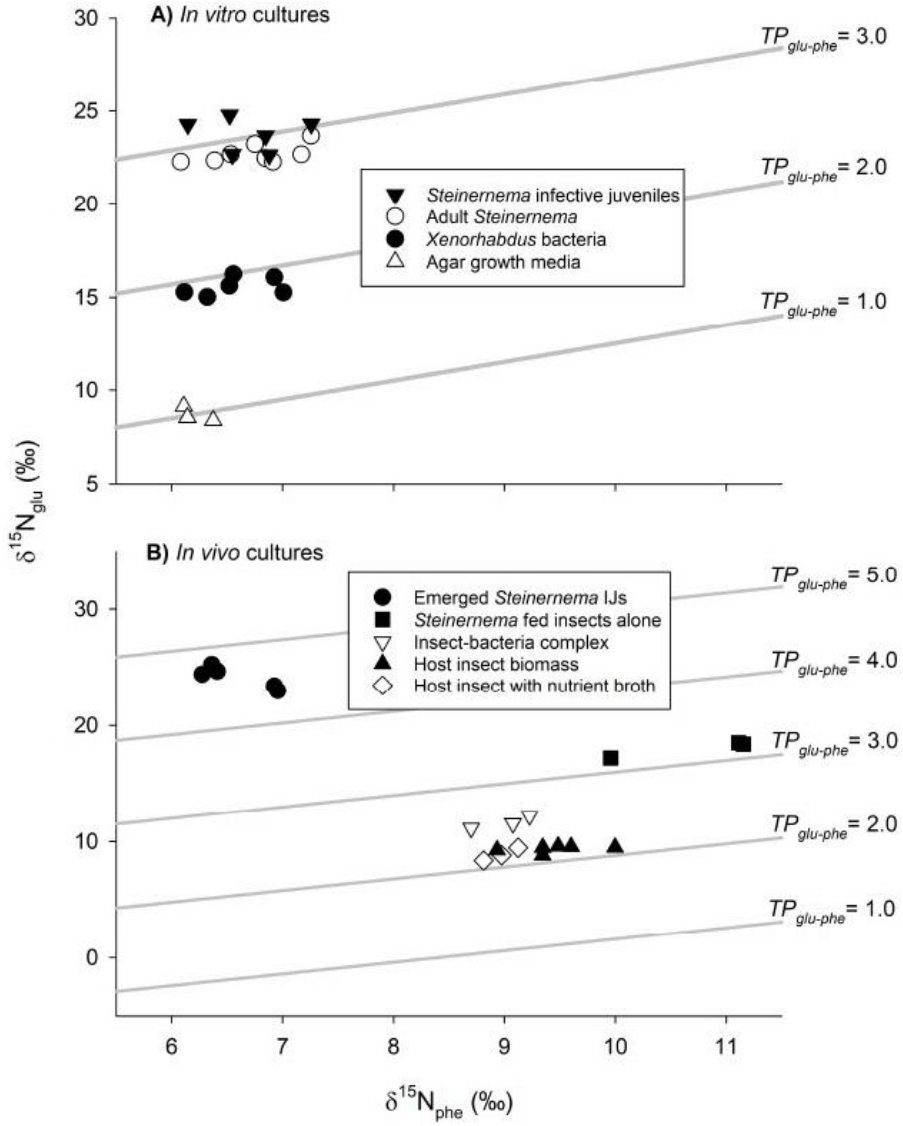

Figure 2: Trophic analyses reveal *Steinernema* nematodes feed on *Xenorhabdus* bacteria A) *In vitro* and B) *In vivo*. Trophic isoclines are represented via numeric $TP_{glu\text{-}phe}$ ‰ ratios. Specific bacterial cultures or animals are displayed as the different shapes shown in the figure legends.

190

191 ***In vivo* trials**

192 These findings allowed for the subsequent *in vivo* trials involving insect cadavers (Fig. 2B, Table

193 1 and File S1). As reported above, the mean $TP_{glu\text{-}phe}$ of an uncolonized insect cadaver was 2.2

194 ± 0.02 (N = 6). When the insect was colonized by bacteria alone, the $TP_{glu\text{-}phe}$ of the insect-

bacteria complex was 2.5 ± 0.03 (*N* = 3). This complex represented the blending of consumer and diet (as described in Steffan, 2017), wherein the consumer (i.e., the *Xenorhabdus* bacterial population) was suffused within and throughout its diet (the insect cadaver). Given that both the bacterial and insect biomass were available within the cadaver, this established the basis for the question as to what a developing nematode would consume/assimilate within the cadaver. The diet of the nematodes (i.e., the insect-bacterial complex) was measured at ~2.5, thus if the nematodes within the cadaver fed randomly on all available substrates, the nematode $TP_{glu\text{-}phe}$ would be expected to be ~3.5 (i.e., ~2.5 + 1.0). However, the infective juveniles emerging from the cadavers registered a $TP_{glu\text{-}phe}$ of 4.6 ± 0.08 (*N* = 5), a full trophic level higher than expected.

Table 1. Summary of *in vitro* and *in vivo* trophic measurements.

Consumer[a]	Diet type[b]	$TDF_{glu\text{-}phe}$[c]	$TP_{expected}$[c]	$TP_{glu\text{-}phe}$[c]
in vitro growth conditions				
None	Yeast-soy lipid agar (YE-YS)	NA	1.0	1.0
Xenorhabdus	Yeast-soy broth (YE-YS)	6.53	2.0	1.9
Steinernema (adults)	*Xenorhabdus* on yeast-soy lipid agar (YE-YS)	6.96	3.0	2.9
Steinernema (IJs)	*Xenorhabdus* on yeast-soy lipid agar (YE-YS)	8.02	3.0	3.0
in vivo growth conditions				
None	*Galleria* (base of food-chain)	NA	2.0	2.2
None	*Galleria* + PBS buffer (positive control)	NA	2.0	2.2
None	Yeast-soy broth (YE-YS)	NA	2.0	2.2
Xenorhabdus (measured as *Galleria-Xenorhabdus* complex)	*Galleria*	NA	2.5	2.5
Steinernema IJs	*Galleria-Xenorhabdus* complex	NA	3.5	4.6

[a]Each organism in the ecosystem was assessed for its trophic position as a consumer under controlled *in vitro* conditions or *in vivo* within an insect cadaver. None indicates that the condition tested was diet only, no consumer.

The data above demonstrated that adult *Steinernema* nematodes consume their mutualistic bacteria. During this stage, *Xenorhabdus* bacteria colonize the anterior intestinal caecum. To determine if this colonization influences the ability of *Steinernema* nematodes to consume *Xenorhabdus*, the $TP_{glu\text{-}phe}$ of adult *Steinernema* cultivated on lawns of either wild type *Xenorhabdus*, or a non-colonizing mutant (Δ*SR1*) was assessed {Cowles, 2008}. Nematodes had the same $TP_{glu\text{-}phe}$ regardless of the colonization proficiency of the bacterial diet, indicating that colonization is not required for nematode direct feeding on its symbiotic bacteria (File S1).

X. nematophila **transcriptional control of metabolic pathways**

The trophic analyses described above establish *X. nematophila* bacteria as the linchpin organism in the closed ecosystem, responsible for direct consumption of the insect tissue and serving as a primary food source for its mutualistic host *S. carpocapsae*. To gain insights into the metabolic pathways utilized by *X. nematophila* in performance of these functions, the global regulons of several transcription factors was determined using an exploratory microarray analysis, portions of which have been reported elsewhere (Fig. 2 and Table S1, and File S2) {Lu, 2011; Lu, 2012; Chaston, 2011; Hussa, 2015}. Microarray analyses were conducted on mutants lacking genes encoding the transcription factors LrhA, RpoS, NilR, and Lrp, each of which has a defect in one or more aspects of the *X. nematophila* life cycle {Vivas, 2001; Cowles, 2006; Cowles, 2007; Richards, 2008}. In addition, since the primary to secondary form phenotypic variation globally influences host-interaction phenotypes, the transcriptional profiles of these variants were examined from a metabolic perspective. The mutant and secondary form cells were each compared to their wild type parent or primary form, respectively, using a 2<|fold change| significance cutoff for differences in transcript levels.

The number of differential transcripts are a fraction of the 3733 averaged total expressed chromosome ORFs among the strains. The number of genes with differential transcript abundance in mutant/secondary form compared to wild-type/primary was highest in Δ*lrhA* at 396 genes (10.6%), followed by Δ*lrp*, secondary form, Δ*rpoS*, and Δ*nilR* with 273 (7.3%), 159 (4.3%), 157 (4.2%), and 83 (2.2%) differentially abundant transcripts, respectively (Fig. 2A). The proportion of genes categorized as being involved in metabolic activity varied amongst the strains. Through KEGG annotation, the highest proportion of differentially-expressed genes categorized as metabolic was observed in the Δ*rpoS* strain, at 38.9%, with Δ*lrhA*, Δ*lrp*, secondary form, and Δ*nilR* having metabolic-related activities at 18.9%, 13.6%, 10.7%, and 9.8%, of the differentially expressed genes in the respective strain. Differential transcript overlap was observed while comparing the 5 strains (Supplemental figure 1). The largest overlap

between 2 strains was for the secondary form and Δ*lrp* mutant, consisting of mostly amino acid (*xncB*, the aminotransferase XNC1_2154) and lipid biosynthesis (*fabG*, *xncL*) genes. *X. nematophila* lacking *lrp* are phenotypically secondary form {Cowles, 2007}. Another large overlap was observed between Δ*lrp* and Δ*nilR*, which synergistically repress nematode colonization {Cowles, 2006}. The overlap regulation includes the phosphotransferase system/ascorbate metabolic (XNC1_2826-2828) genes and prokaryotic defense system genes (XNC1_3717-3719, 3724, and 3931).

Functional analysis of the differentially expressed metabolic transcripts was performed through KEGG annotation using BlastKOALA (KEGG Orthology and Links Annotation). Sequences were aligned against a nonredundant set of prokaryotic KEGG genes using BLAST searches (Kanehisa, 2016). Consistent with the KEGG annotation analysis noted above, of the strains tested Δ*rpoS*, Δ*lrhA*, Δ*lrp* were the most strongly impacted with respect to metabolic pathway transcripts. These three strains displayed differences in carbohydrate and amino acid metabolic regulation (Fig. 2A). Branches of carbohydrate metabolism, like propanoate, pentose and glucuronate, and glyoxylate metabolism were impacted by the Δ*lrhA* and Δ*rpoS* mutations (Fig. 2B). Inositol phosphate metabolism was impacted in Δ*rpoS* and Δ*lrp* strains, while pyruvate metabolism was impacted in the Δ*lrhA* strain. Butanoate metabolism, a branch of carbohydrate metabolism where the amino acid ornithine is converted into short-chain fatty acids, was commonly interrupted for all mutant strains except Δ*nilR*. Amino acid biosynthetic pathway transcripts were differently regulated between these three strains, with tyrosine, and the alanine, aspartate, and glutamate biosynthetic pathways similarly disrupted. Histidine and valine metabolism was uniquely altered by the Δ*rpoS* mutation, glycine, serine, and threonine metabolism was uniquely altered by the Δ*lrhA* mutation, and phenylalanine metabolism was uniquely altered by the Δ*lrp* mutation. To investigate the impacts these pathways and others

have on the *Xenorhabdus*-*Steinernema* lifecycle, a time course metabolomics experiment was designed to measure the relative quantities of metabolites within them.

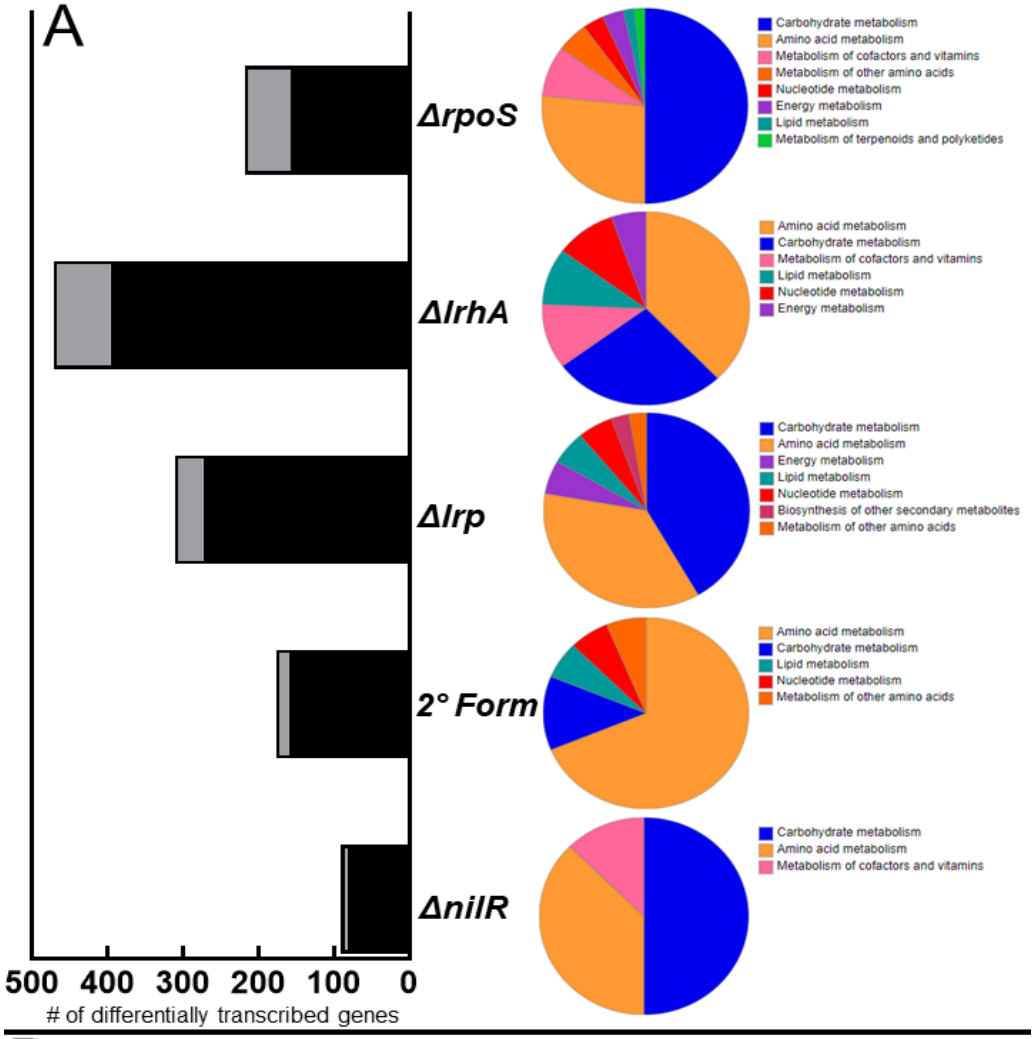

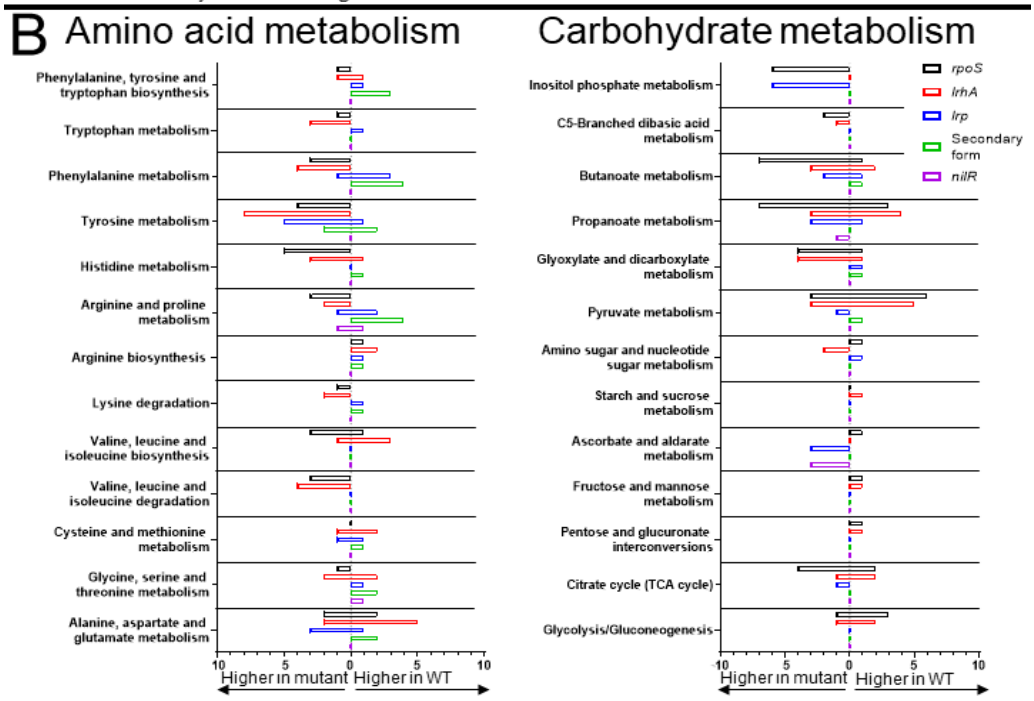

268

Figure 2: Differentially expressed transcripts between *X. nematophila* mutants and their broad functional categorization. A) Quantification of the number of differentially regulated transcripts and how many are considered metabolic (light grey), as determined by KEGG annotation. |Signal fold change| > 2 was used as a cutoff for significance. BlastKOALA functional categorization of the differential metabolic transcripts are adjacent. The color legend is organized by having the most common category listed first. B) Breakdown of the specific amino acid and carbohydrate metabolism pathways that were affected by the mutations, compared among each strain, with # of genes listed. Positive genes represent transcripts higher in the mutant relative to WT, negative genes represent transcripts lower in the mutant relative to WT.

The metabolomic profile of EPNB-infected *G. mellonella*: an overview

Having established that *X. nematophila* bacteria consume infected insect tissue, and in turn the bacteria are consumed by reproducing and developing nematodes, the temporal dynamics of metabolic profiles associated with these processes were examined. *G. mellonella* were infected with *S. carpocapsae* infective juveniles colonized by *X. nematophila* bacteria. Weights of the whole insect samples were relatively similar (Table S2). Insects were sampled over a 16-day time-course. As expected, insects began to die by Hour 24 after infection, and both living and dead insects were sampled at that time point. *X. nematophila* will have reproduced rapidly in order to suppress the insect immune response and release toxins to kill the insect host. By the second day post-infection all insects had succumbed to infection and were dead. Consistent with the initial degradation of the insect cadaver by bacteria predicted by the trophic analysis conducted above, the nematodes began to reproduce by Day 4, 3 days after the insects had died from infection (Fig. 3). At Day 7 post-infection, insect cadavers were placed in a collection trap to encourage the emergence of progeny *S. carpocapsae* IJs. Adults and IJs were observed at this stage. This is when the 2nd generation of nematodes begin to emerge, and endotokia matricida is occurring when some of these juveniles will consume their parents for nutrients. By Day 16 the insect cadavers were largely consumed, and most

287 remaining IJs will have exited. On Day 16 the *S. carpocapsae* IJs, colonized by *X. nematophila*
288 symbionts, were collected from the water trap and analyzed with the other samples. The
289 proportions of nematodes observed at these stages are consistent with previous observations,
290 in which there are more adults and juveniles during the middle phase compared to IJs which
291 changes to high numbers of IJs into the late phase {Cao, 2020}. The above observations led us
292 to design a time course metabolomics experiment in which samples were divided into 3 major
293 time frames: the early infection, characterized by bacterial replication and the killing of the insect
294 host, middle infection, characterized by nematode reproduction and nutrient conversion of the
295 cadaver, and late infection, characterized by nutrient depletion and IJ emergence.

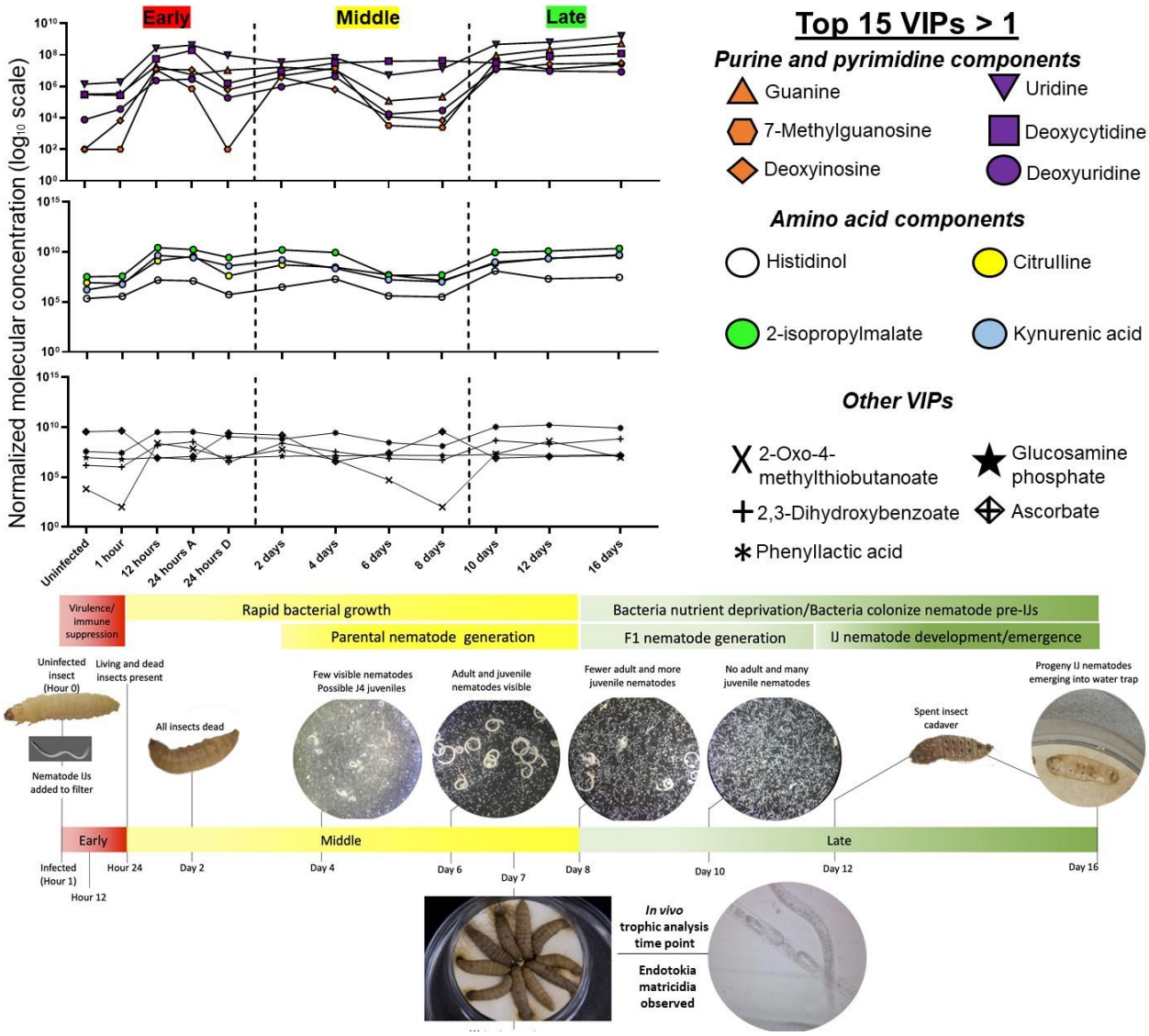

296

297 **Figure 3: Key moments in the EPNB lifecycle mapped onto important molecules are**
298 **indicative of the bioconversion of the insect cadaver.** The top 15 VIPs>1 metabolites
299 averaged relative abundances were grouped together into 3 categories: purine and pyrimidine
300 components, amino acid components, and other important molecules. Relative metabolite
301 abundance in log scale is displayed on the y-axis of the line graphs.

302

Metabolites were extracted from individual insects sampled over the infection time course and analyzed using an untargeted UHPLC-HRMS method. The untargeted metabolic profiling analysis revealed 13,748 spectral features. Through the mass spectrometric measurements, a total of 170 of these features were identified based on comparison to known exact mass-to-charge (*m/z*) ratio and retention times from a database of central energy metabolites (File S3). Another 3,138 unidentified spectral features were included in the analysis and putatively annotated based on their exact masses compared to a *Xenorhabdus* secondary metabolite database (File S4). This database serves as a rich repository to explore secondary metabolite temporal flux in the tripartite ecosystem of insect, bacteria, and nematode.

Multivariate data analysis shows metabolic profile gradient corresponding to infection progression

Partial least squares-discriminant analysis (PLS-DA) was performed to observe gross chemical environment changes over time of insect bioconversion to nematode-bacterium complex, when combining all detected metabolite data. A three-dimensional PLS-DA plot shows a progression of distinct metabolic profiles from uninfected insects (black circles) to insects in which bacteria and nematodes are reproducing (red and yellow gradients), and finally to fully consumed insects (green gradients) from which bacterial-colonized infective juvenile populations are emerging (Fig. 4A). Component 1 is 41.1% and contributes the most significantly to the separation observed in the PLS-DA plot.

To examine which metabolites are responsible for most of the variation represented by the PLS plots, Variable Importance in Projection (VIP) values for component 1 were calculated. VIP is a weighted sum of squares of the PLS loadings that considers the amount of explained Y-variation in each dimension. A VIP score >1 indicates that the metabolite significantly contributed to time point differentiation. Most of the VIP>1 metabolites exhibited a bimodal pattern, going from very low in the uninfected insect, to rising in the early bacterial replication

phase, to dropping during the middle nematode reproduction phase, and finally rising very high in the late nutrient deplete phase (Fig. 4B and File S5). Overall, these metabolites were involved in nucleotide and nucleoside biosynthesis, NAD^+ biosynthesis, and iron acquisition. These included the purine and pyrimidine metabolites 7-methylguanosine, guanine, deoxyinosine, uridine, deoxyuridine, and deoxycytidine. Other top metabolites include kynurenic acid and anthranilate which are precursors to NAD^+ synthesis. Of the top 15 VIPs, ascorbate was the only molecule to exhibit a decreased abundance over time, dropping from very high abundance to very low later in the time course. This vitamin is necessary for neuron development and could be salvaged from the cadaver to build the nematode nervous systems {May, 2012}.

Kynurenic acid is an intermediate in the kynurenine pathway and is a way for organisms to synthesize NAD^+ if they cannot *de novo* synthesize the compound through encoding a quinolinate phosphoribosyltransferase (QPRTase) {Katsyuba, 2018}. *S. carpocapsae*, like *C. elegans*, lacks a standard QPRTase but encodes the uridine monophosphate phosphoribosyltransferase (*umps-1*) which synthesizes NAD^+ from the kynurenine pathway {Rougon-Cardoso, 2016; Lee, 2020}. Significant flux of this metabolite throughout the lifecycle could be a metabolic signature nematode NAD^+ production.

Phenylacetic acid is a uremic toxin that builds up in kidney patients and is the product of bacterial metabolisms. In *P. aeruginosa* phenylacetic acid (PAA) accumulates at high cell density and inhibits the Type III Secretion System (T3SS), which is toxic to host cells {Wang, 2013}. *X. nematophila* does not have a T3SS but does have the evolutionarily related flagellar export apparatus. The transcription factor Lrp positively regulates the flagellar regulon, as well as the gene encoding the XlpA lipase, an enzyme associated with the ability of *X. nematophila* to support *S. carpocapsae* reproduction {Richards, 2008; Richards, 2010}. Although not detected by microarray analysis, quantitative reverse transcriptase analyses indicate that the transcription factor LrhA also positively regulates *xlpA* expression {Richards, 2008}. The

353 relatively higher intensity of phenylacetic acid at later stages of insect bioconversion may signal
354 inhibition of secretion of bioconversion enzymes.

355 2,3-dihydroxybenzoate is a compound involved in siderophore biosynthesis non-
356 ribosomal peptide biosynthesis of siderophore, highlighting a potential importance in iron
357 acquisition from the cadaver. Iron itself does not appear to be limited in the cadaver but it needs
358 to be harvested by the bacteria to aid in nematode reproduction {Ciche, 2003}. *X. nematophila*
359 does not encode *entA* or *entB*, genes that participate in the conversion of 2,3-
360 dihydroxybenzoate to the enterobactin siderophore pathway {Latham, 2014}. Siderophore
361 production is necessary for antibiosis in the closely related *Photorhabdus-Heterorhabditis* EPNB
362 symbiosis, which has characterized *phb* genes that are homologous to the *ent* genes {Ciche,
363 2003}. The *Photorhabdus phb* genes encode proteins that sequester iron from the cadaver to
364 fend off soil-dwelling bacterial colonizers that exploit the cadaver, and *X. nematophila* does not
365 have any homologs to these genes. *X. nematophila* does not completely dominate the bacterial
366 community of the insect host, suggesting that other taxa such as *Alcaligenes* are possibly
367 responsible for this concentration shift {Cambon, 2020}.

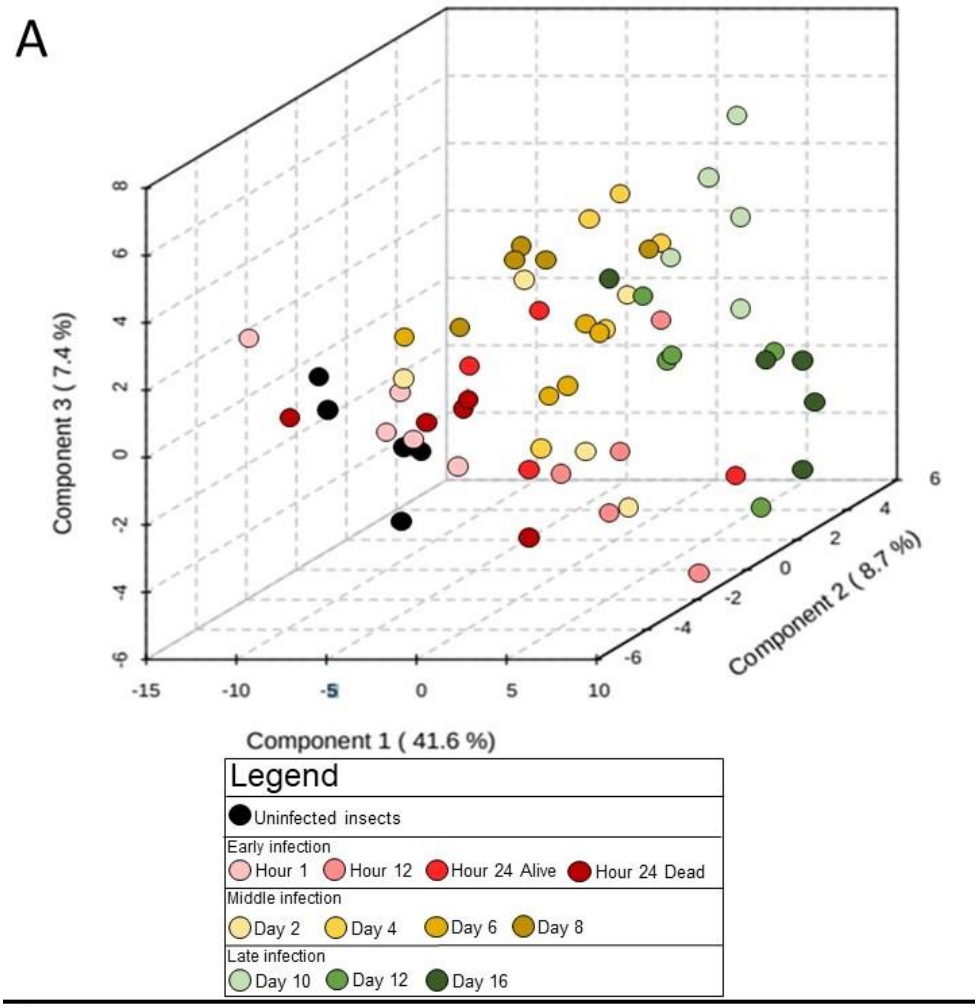

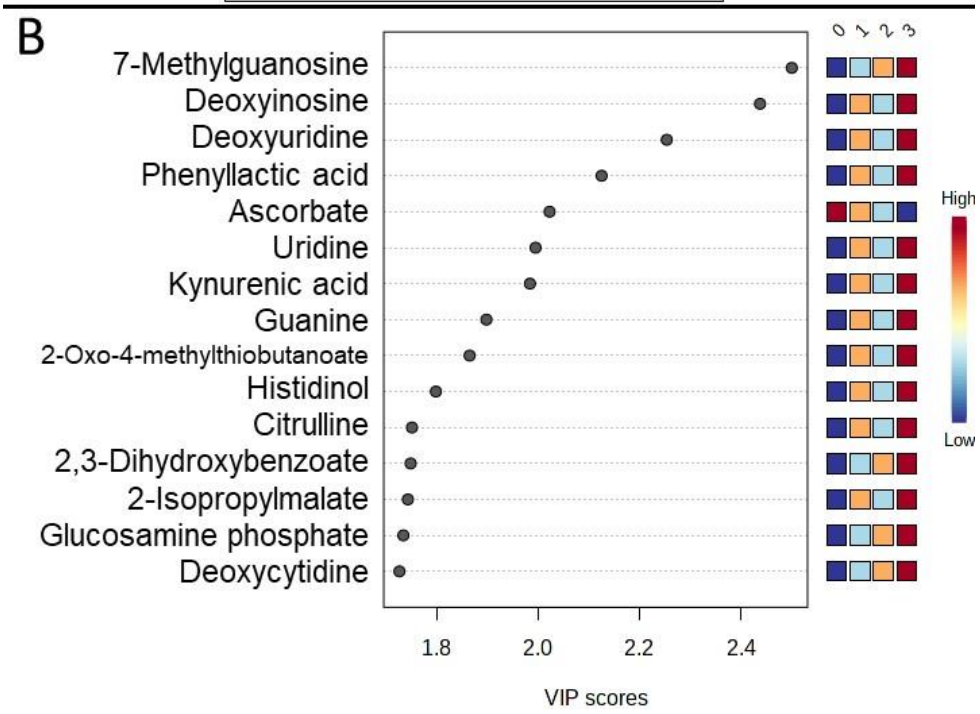

368

Figure 4: Distinct chemical environments occur during bioconversion of an insect cadaver by *S. carpocapsae* and *X. nematophila*. A) Three-dimensional partial least squares-discriminant analysis (PLS-DA) of time course infection metabolic profiles grouped according to stage of infection: uninfected (black) and early (red gradient), middle (yellow gradient), and late infected insects (green gradient). Components contributing to the separation of the profiles are listed (in %) on the axes. B) The top 15 VIPs contributing to component 1 are listed, where the relative abundance shifts over the time course shown in a heatmap on the right. The numbers on top of the heatmap show the time phases: 0 (uninfected), 1 (early), 2 (middle), and 3 (late).

To identify patterns and groups of metabolite abundance changes over time, hierarchical clustering was performed to reveal groups of metabolites that exhibit similar concentration changes over the time course of bioconversion. A dendrogram of all 170 identified metabolites was generated using the absolute value of the spearman correlation between molecular concentrations, where distance between molecules is defined as 1-|rs| with rs as the spearman rank correlation between time course data points of said molecules (Fig. 5A). Metabolite concentration averages were taken for the four time-phases defined: uninfected, early, middle, and late infection. Metabolite clusters were visualized in a heatmap that displays their pairwise correlation between each molecule (Supplemental Figure 2). A heatmap that shows the metabolite clusters, separated by black bars, with the molecule trends in concentration change over time was generated (Fig. 5B). There were 10 total metabolite clusters identified, each with a clear molecular concentration pattern in which the metabolites in that cluster exhibited similar rates of change together over the time phases.

Clusters of metabolites that exhibit similar rates of change for each time phase were examined to gain an understanding of very broad metabolic pathways affected at each time phase (File S3). In the early infection phase relative to the previous uninfected phase, there are increased abundances of Clusters 4 and 5. These clusters contain metabolites involved in

glutathione biosynthesis (glutamate, cysteine, pyroglutamic acid, and $NADP^+$). Glutathione intermediates are increasing while glutathione itself (Cluster 3) is decreasing. Decreased abundance of glutathione paired with increased abundance of synthesis intermediates could be indicative of how the insect is fighting off this pathogen; the insect immune response attempts to strike an equilibrium between non-specific reactive molecules released through the phenoloxidase melanization cascade and the antioxidant glutathione which protects against the reactive molecules {Clark, 2010; Stahlschmidt, 2015}. Also increasing during this phase are several amino acids, namely those involved in tryptophan metabolism (tryptophan itself and indole). Metabolites that exhibited continuously decreasing abundances in the early phase relative to the uninfected phase were mapped onto Clusters 1, 3, 8, 9, and 10. These clusters contain many compounds, and the highest proportions are involved in purine and pyrimidine biosynthesis and ascorbate metabolism (myo-Inositol, UDP-glucose, UDP-glucuronate, and glucarate). From the microarray data, generally the regulator mutants caused transcripts in ascorbate (*nilR, lrp*) and tryptophan (*lrhA, rpoS*) to decrease. These data from the early phase represent the clusters of metabolites that could be targeted by the bacteria to induce insect death and the metabolites used by the insect to fight the losing war.

From the early phase into the middle infection phase, few clusters exhibit an increase in rates of change. These metabolites are in Clusters 8 and 10, which contain several purine components (deoxyinosine, xanthosine, and inosine) as well as one of the only B vitamins detected in this screen, riboflavin (vitamin B_2). Other detected B vitamins, like biotin (vitamin B_7), pantothenate (vitamin B_5), and 4-pyridoxate (catabolic product of vitamin B_6), are decreasing in abundance during the middle phase. Many other compounds decreased in abundance during the middle infection phase, relative to the previous early infection phase. These include amino acids (arginine, phenylalanine, tyrosine, tryptophan, cysteine, and methionine), which could reflect that these are the amino acids being incorporated into protein creation for bacterial and

nematode biomass accumulation. Microarray analysis indicates widespread differential regulation in these amino acid categories, particularly in the secondary form, *lrp*, and *lrhA* mutants. Other decreasing compounds include pyrimidine intermediates (UMP, CMP, CDP, and UDP) and ascorbate and sugar acid compounds. These data from the middle phase are reflective of the compounds that are being syphoned from the cadaver and incorporated into the nematode lifecycle.

As the insect cadavers entered the late infection phase, nucleic acids (guanine, thymine, and uracil) and amino acids (arginine, cysteine and methionine, and aspartate) steeply increased. This suggests these accumulating compounds are available for nematode DNA, RNA, and protein incorporation, but other factors such as overcrowding in the cadaver or lack of other necessary resources force the nematode to exit. Decreasing rate of change of metabolites relative to the previous middle phase included compounds involved with leucine metabolism and the TCA cycle. These could be more rate-limiting compounds, where their decreasing abundance could signal to the expanding nematode population that it is time to exit.

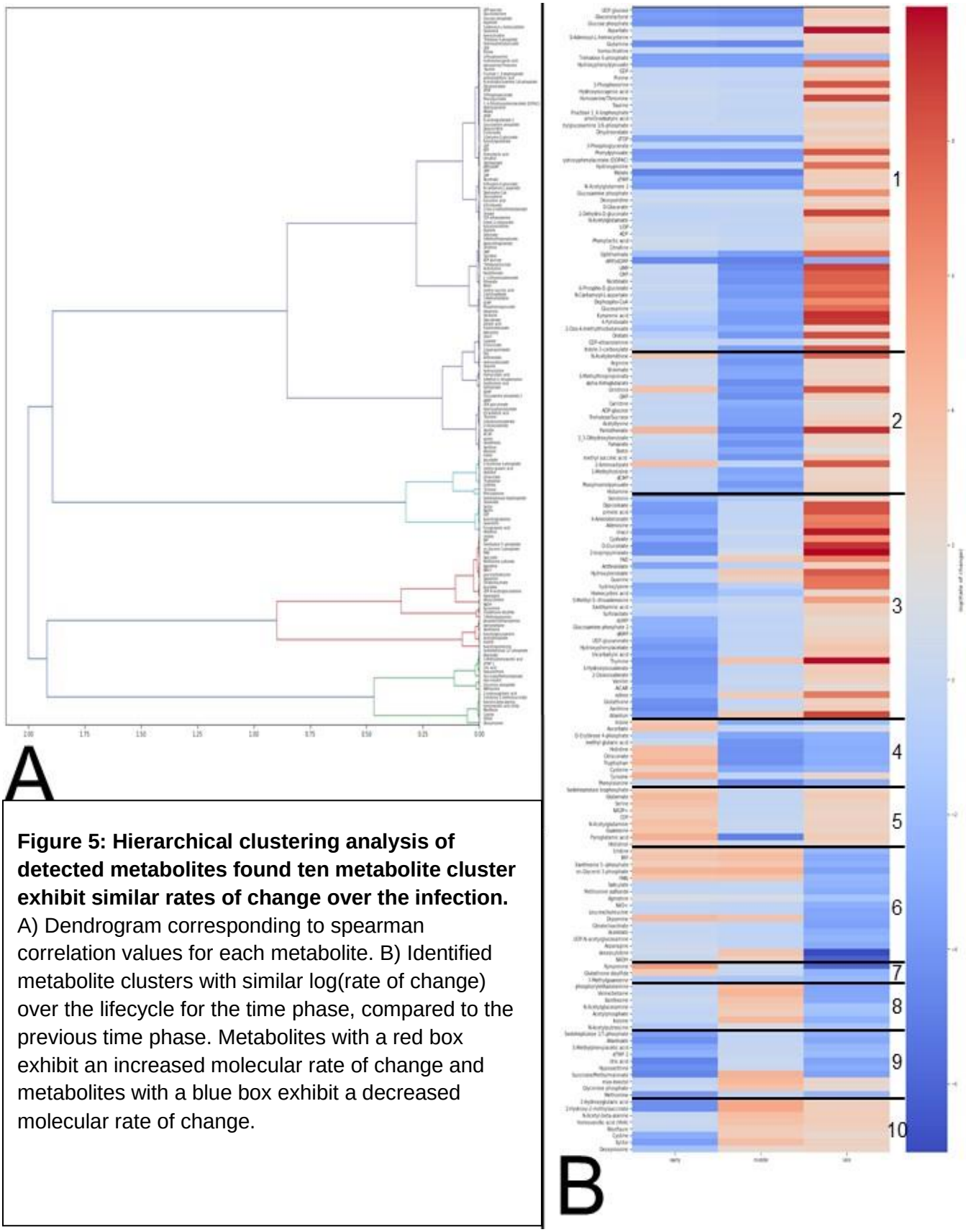

Figure 5: Hierarchical clustering analysis of detected metabolites found ten metabolite cluster exhibit similar rates of change over the infection. A) Dendrogram corresponding to spearman correlation values for each metabolite. B) Identified metabolite clusters with similar log(rate of change) over the lifecycle for the time phase, compared to the previous time phase. Metabolites with a red box exhibit an increased molecular rate of change and metabolites with a blue box exhibit a decreased molecular rate of change.

433

Interference of insect tricarboxylic acid (TCA) cycle is critical for infection success and subsequent propagation of nematodes

To identify significant metabolites that are important for infection progression, an ANOVA with post-hoc Tukey's HSD test was performed on metabolite abundances throughout the lifecycle. Two comparisons were examined: metabolite abundances from uninfected insects compared to individual time points, and individual time points compared to the next subsequent time point. As summarized in Figure 6, TCA cycle components significantly (p<0.05) fluctuate in relation to uninfected insects as well as between time phases, throughout the time course.

In the early phase of infection, while the insect is still alive and combatting bacteria and nematode invaders using innate immunity, several key TCA cycle intermediates are reduced in abundance relative to an uninfected insect (Fig. 6). This is shown through significantly decreased abundances of citrate in the Hour 12 and Hour 24 living insects compared to the uninfected insect and the Hour 24 dead insects. Although not significant, a similar trend is observed for two other TCA-related metabolites, malate and *sn*-glycerol-3-phosphate, which aids in NAD^+ regeneration through the glycerol phosphate shuttle, as well as NAD^+, NADH, fumarate {Shi, 2018}. This could mean these metabolites were diverted for the immune response, given the differences between the living and dead insects. As the infection progresses into a middle phase, citrate abundances flux, but generally are decreasing. Into the late phase on Day 10, malate, *sn*-glycerol phosphate, succinate, and citrate all drop, which could suggest carbon is being stored (rather than used) in the IJs before they exit the cadaver.

TCA cycle components were mostly in Cluster 6 (*sn*-glycerol-3-phosphate, NAD^+, NADH, citrate and isocitrate) and Cluster 2 (fumarate, alpha-Ketoglutarate). Student t-tests were utilized to determine additional significant components by comparing each broad time phase to the uninfected insects (File S3). Acetylphosphate was found to be approaching significantly high (p<0.1) at the early phase and was significantly high (p<0.05) at the middle and late phases.

459 NAD^+ was found to be approaching significantly low (p<0.1) at the early and middle phases and
460 was significantly low (p<0.05) for the late phase. *Xenorhabdus* spp. cannot synthesize NAD^+
461 and requires nicotinate for growth {Orchard, 2004; Martens, 2005}. Generally, the trend for all
462 TCA components in the lifecycle seem to be decreasing as the infection progresses with the
463 exceptions of acetylphosphate, FAD, and succinate.

464

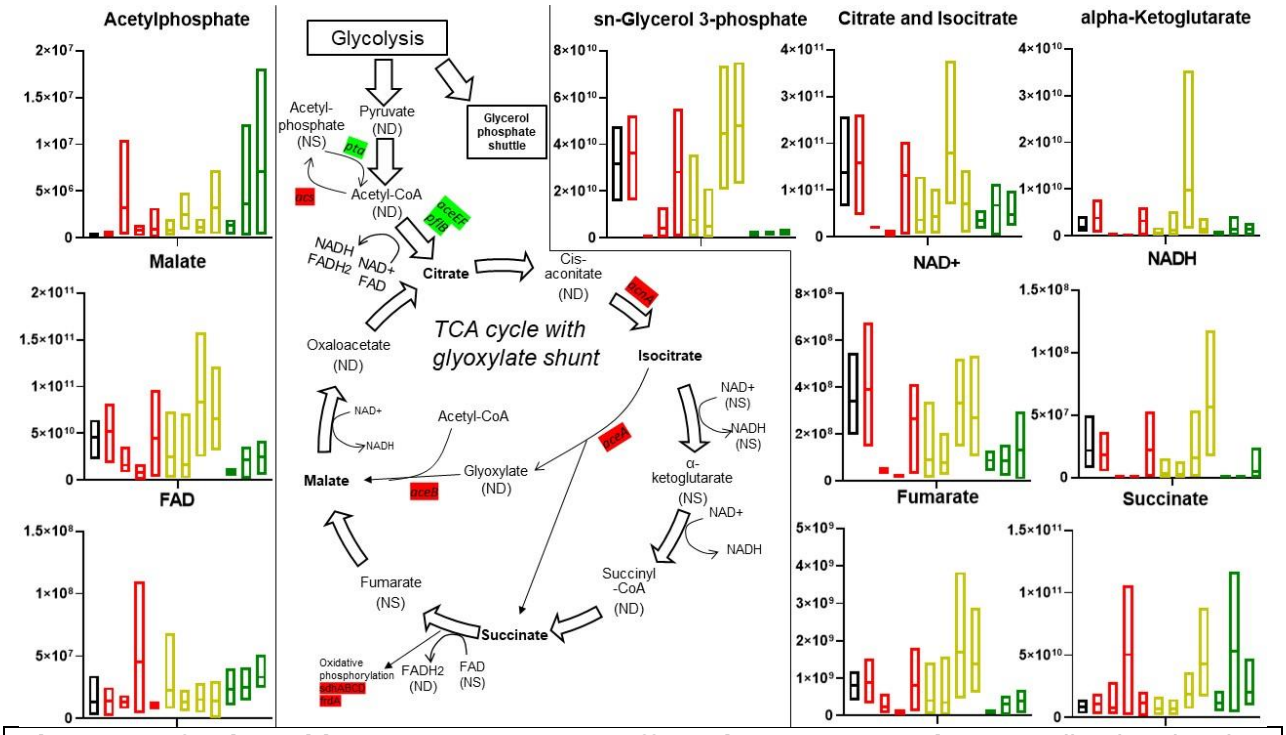

465 **Figure 6: Infection with *S. carpocapsae* IJs affects insect TCA cycle.** Normalized molecular
466 concentration box plots throughout the lifecycle are shown for all detected metabolites involved
467 in the TCA cycle. Box plot colors represent which time phase the individual plots belong to for:
468 uninfected (black), early infection (red, going from earliest, 1hr, to latest, 24 hours dead, time
469 points), middle infection (yellow, days 2-8), and late infection (green, days 10-16). Lines in the
470 middle of the boxes indicate the mean molecular concentration. Bolded metabolites indicate
471 significant concentration shifts during the life cycle. NS indicates detection, but not significantly
472 affected (through the ANOVA) throughout infection. ND indicates not detectable. Highlighted

genes were detected as significant for the microarray in the Δ*lrhA* and Δ*rpoS* strains. Green indicates positive regulation, red indicates negative regulation.

The aforementioned *X. nematophila* mutants experienced differences in transcripts involved in either pyruvate metabolism, glyoxylate metabolism, or the TCA cycle (File S2). Most of these genes were regulated in the Δ*lrhA* and Δ*rpoS* mutant backgrounds. *aceA* and *aceB* are negatively regulated, while *aceE* and *aceF* were positively regulated between Δ*lrhA* and Δ*rpoS* mutant strains and WT. These genes are involved in the glyoxylate shunt which is a pathway utilized by many bacteria and nematodes to convert 2-carbon compounds into energy resources, in the absence of bountiful sugars {Maloy, 1982}. Δ*rpoS* mutants upregulate several succinate dehydrogenase genes which are necessary for oxidative phosphorylation. In *E. coli* these genes are regulated in response to different environmental conditions like iron and heme availability {Park, 1995}.

Acetyl-coA is an important node in metabolism, connecting glycolysis, the TCA cycle, fatty acid, amino acid, and secondary metabolite pathways, and acetate dissimilation {Wolfe, 2015}. RpoS and LrhA positively influence the expression of AceF, PflB, Pta, and AckA. Pta-AckA comprise the acetate dissimilation (excretion) pathway {Wolfe, 2015}. Coordinated elevation of these enzymes is predicted to result in lower levels of acetyl-coA and higher levels of acetylphosphate and acetate, which is excreted and available for use by the nematodes. Acetylphosphate is a phosphoryl donor for some response regulators and can be a donor for protein acetylation. Protein acetylation, a ubiquitous post-translational modification in prokaryotes and eukaryotes, is involved in regulation of many different bacterium-host interactions like chemotaxis, replication, and acid resistance, as well as regulating bacterial DNA-binding and protein stability {Ren, 2017}. Acetylphosphate was detected in the metabolome and generally increased over the infection, as well as being a VIP>1 metabolite for components 1 and 2. Acetate freely diffuses across membranes and can be incorporated into

biomass of both bacteria and nematodes via the glyoxylate shunt {Alaimo, 2012}. *pflB* is predicted to encode the pyruvate-formate lyase (PFL) enzyme involved in conversion of pyruvate and CoA into formate and acetyl-coA and is greatly (>7 |fold change|) downregulated in the Δ*rpoS* and Δ*lrhA* mutants relative to wild type. PflB converts glucose to formate, and up to one-third of the carbon procured from glucose is converted through this enzyme in *E. coli* {Doberenz, 2014}. PFL condenses acetyl-CoA and formate, allowing for the microbes to use acetate and formate (fermentation products) as the sole carbon sources {Zelcbuch, 2016}. RpoS and LrhA negatively regulate Acs, which is the acetate assimilation pathway {Wolfe, 2015}. In *E. coli*, Acs activity is inhibited by acetylation of a conserved lysine and its abundance is negatively regulated by the small RNA SdhX {You, 2014; De Mets, 2019}. RpoS and LrhA also both negatively regulate the TCA cycle enzymes AcnA and AceAB, and this inhibition is predicted to result in accumulation of citrate. Citrate and isocitrate progressively decrease in abundance over the infection cycle and these combined data might indicate that citrate produced and accumulated by *X. nematophila* bacteria may be a provision for nematodes, consumed during reproduction.

Analysis of amino acid abundances found proline fluctuates throughout the infection

The amino acid pyroglutamic acid, which is a precursor to glutamate, significantly rises (as determined through the aforementioned ANOVA tests). in abundance during the late phase, at Day 16 compared to the uninfected insect and between Day 12 and Day 16. Glutamate is a precursor for proline metabolism {Watford, 2008}. Proline abundances fluctuated significantly throughout the time course. Compared to uninfected insects, proline levels were significantly lower at Day 10 and higher at Day 16, but otherwise were not significantly different. When comparing each time point to the previous, there was a significantly higher level of proline in dead insects at Hour 24 relative to living insects at the same time point. However, in dead

523 insects between Hour 24 and Day 2 the levels of proline dropped again. Thereafter there was a
524 cycle of increase and decrease in proline abundance (Day 4<Day 6, Day 8>Day 10, Day
525 12<Day 16), with an overall rise throughout the middle and late phases. Additional metabolites
526 in the arginine/proline/polyamine metabolism pathways that were significantly different among
527 samples based on student t-tests (File S3), included ornithine, which was significantly high at
528 the early and middle infection stages compared to uninfected insects, and hydroxyproline, which
529 was significantly high at early, middle, and late infection stages compared to uninfected insects.
530 Hierarchical clustering analysis reveals Cluster 1 (proline and hydroxyproline) and Cluster 5
531 (glutamate and pyroglutamic acid) contain these compounds. These cluster trends differ in the
532 early phase, where Cluster 1 decreases while Cluster 5 increases, possibly indicating that these
533 compounds are getting converted into each other.

534 Microarray analysis of Δ*lrhA*, Δ*lrp*, Δ*nilR*, Δ*rpoS*, and secondary form *X. nematophila*
535 mutants reveal similarities to each other in disrupted proline gene regulation compared to their
536 wild type/primary form counterparts. *putA*, predicted to encode 1-pyrroline-5-carboxylate
537 dehydrogenase, an enzyme involved in the conversion of proline to glutamate, was negatively
538 regulated (2<|fold change|) in the *ΔlrhA* and *ΔrpoS* strains, and positively regulated in the
539 secondary form strain. PutA is necessary for virulence in *Pseudomonas aeruginosa* and
540 protects the bacterium against oxidative stress {Zheng, 2018}. XNC1_2468 is downregulated in
541 the Δ*lrp*, Δ*rpoS*, and secondary form mutant backgrounds. This gene encodes a spermidine N1-
542 acetyltransferase as part of polyamine biosynthesis from ornithine and putrescine. XNC1_2274
543 and XNC1_3619 are FAD-dependent oxidoreductases involved downstream of proline
544 metabolism in putrescine utilization and are upregulated in the Δ*lrhA*, Δ*lrp*, Δ*nilR*, and Δ*rpoS*
545 mutant backgrounds. These genes are mostly involved in downstream proline metabolism,
546 specifically polyamine biosynthesis. Pathogenic gram-negative bacteria exploit polyamine-
547 related processes of their host for growth and proliferation, using these host molecules for toxin

548 activity, biofilm production, and limiting host immune responses {Shah, 2008; Di Martino, 2013}.
549 XNC1_2154 is predicted to encode an enzyme with L-aspartate:2-oxoglutarate
550 aminotransferase activity and is downregulated in the secondary form and Δ*lrp* mutant
551 backgrounds.

552 Amino acids leucine, isoleucine, and phenylalanine amino acids were significantly higher
553 in abundance at the late stage of infection. These are essential amino acids which *C. elegans*,
554 and presumably *S. carpocapsae*, must acquire from its diet (i.e. bacteria) {Zečić, 2019}. Several
555 *X. nematophila* genes, including *ilvC* and *ilvI*, involved in leucine/isoleucine biosynthesis were
556 differentially regulated in the Δ*lrhA* (negatively) and Δ*rpoS* (positively regulates *ilvC* and
557 negatively regulates *ilvI*) mutant backgrounds, relative to wild type. Δ*rpoS* mutants had higher
558 levels of *leuA* transcript, a gene predicted to encode a 2-isopropylmalate synthase, a leucine
559 precursor which is increases throughout the lifecycle. Δ*lrhA* increased transcript abundances of
560 *fadA, fadB*, *fadI,* and *fadJ* which participate in the conversion of leucine and isoleucine into fatty
561 acids and acetyl-CoA. In the Δ*lrp* and Δ*rpoS* mutant backgrounds, *mmsA* was upregulated,
562 another gene that encodes a methylmalonate-semialdehyde dehydrogenase that participates in
563 the breakdown of leucine and isoleucine.

564

565 **DISCUSSION**

566 A comprehensive framework to understand how metabolism shifts during infection
567 lifecycles of entomopathogenic nematodes was established. Physiologically, it was examined
568 that *X. nematophila* bacteria consume insect tissues, while *S. carpocapsae* nematodes
569 consume bacteria. The high $TP_{glu\text{-}phe}$ of 4.5 observed in the nematodes emerging from an insect
570 cadaver suggests the IJs were potentially cannibalizing previous generations of nematodes
571 and/or feeding upon bacteria that were, themselves, already feeding on previous generations of
572 nematodes and bacteria, since if the colonizing nematodes were feeding on bacterial and insect

biomass only, they would register at around 3.5 Thus, this high trophic level suggests either endotokia matricida (or bagging) in which nematode eggs hatch within and consume the mother. likely during the second generation of nematodes when nutrients are becoming depleted, or that some other form of cannibalism is occurring within the cadaver {Baliadi, 2004}. A $TP_{glu\text{-}phe}$ of 4.6 is similar to many apex predators, such as large marine carnivores or the rare top predators observed in terrestrial ecosystems {Chikaraishi, 2011; Chikaraishi, 2014; Steffan, 2013; Ohkouchi, 2017}. This underscores the importance of including microbes in studies of organismal trophic identity. In effect, the cadavers used in this study may represent microcosms of the broader communities and ecosystems in which they are embedded. The insect cadavers were, when alive, herbivores. To find multiple levels of carnivory within a single cadaver suggests that a nematode-colonized arthropod mirrors the trophic richness of the broader food-web. The interdigitation of microbial carnivores in a trophic hierarchy—here, nematodes and bacteria—is likely a much more common feature of food-webs than previously thought {Steffan, 2017, Steffan and Dharampal, 2019}. The microbial trophic identities reported in this study may necessitate a re-calibration of organismal niche concepts, but in so doing, will facilitate the unification of the macro- and microbiome in food web ecology.

It should be emphasized that it has been exceedingly uncommon to find higher-order consumers (TP > 4.0) in a community or ecosystem, given that apex predators feed upon other predators that have, themselves, had to find and subdue ‘lower’ carnivores {Lindeman, 1942}. In classical food web ecology, apex predators are generally considered to be large, fierce, and rare vertebrates Elton, 1927, Colinvaux and Barnett, 1979}. However, perhaps the assumption that apex predators exist only within the province of large/fierce/rare vertebrates needs to be revisited. The high trophic positions exhibited by the nematodes in this study suggest that such obligate higher-order consumers are more common than previously thought, with multitudes of apex carnivores existing underfoot in many terrestrial ecosystems. Further, the nematodes can

598 be viewed as farming their symbionts: acting as shepherds that bring their bacterial flock to a
599 fresh insect pasture for harvesting of nutrients.
600 The trophic study established the foundation to understand metabolic shifts occurring in
601 the cadaver. The time course metabolomics study sought to better understand the process of
602 bioconversion in the cadaver, how is the insect biomass being converted to bacterial and
603 nematode biomass? Applying multivariate statistical tests to the infection metabolomics data set
604 revealed distinct time phase clustering. The variance among the time phases seems to increase
605 as infection progresses, as the healthy insects degrades into bacteria and nematode tissue.
606 Nematode IJ samples were also compared to these time phases. These samples form a distinct
607 cluster away from the other time phases (File S5). The IJ samples completely removed from the
608 lifecycle seem to have metabolic profiles most similar to the late time phase, which are insect
609 samples bursting with nematodes (Fig. 3). However, it is important to note that these are input
610 IJs that have spent weeks outside of an insect cadaver. Reassessing this analysis with output
611 IJs that are recently from the nematode is important to follow up on.
612 Metabolic analysis revealed TCA cycle components were among the most significant
613 results, indicating that their use by the entomopathogenic nematodes is paramount to infection
614 success and subsequent nematode propagation. Citrate metabolism is ubiquitous in many
615 intracellular pathogens and has been found to be involved in regulating virulence {Martino,
616 2018}. Citrate is necessary for virulence and growth of the Gram-negative pathogenic bacteria
617 *Pseudomonas aeruginosa*, where NADH levels were reduced when the bacterium was treated
618 with citrate and host-killing activity was abolished as a result {Perinbam, 2020}. This group
619 hypothesized that this could be due to decreased flux through the glyoxylate bypass, which has
620 been found to activate the T3SS in this system {Chung, 2013}. As mentioned, *X. nematophila*
621 does not encode a T3SS, but does have the evolutionarily related flagellar export apparatus.
622 Several *X. nematophila* glyoxylate bypass genes, were differentially transcribed between
623 avirulent genetic mutants and WT. Glyoxylate was not detected in our screen, and whether flux

through this pathway affects virulence should be investigated further. The significant flux of TCA metabolites during the middle phase may be indicative of the role of the TCA cycle in *S. carpocapsae* development, as the TCA cycle has been shown to be essential in early embryogenesis in *C. elegans* {Rahman, 2014; Hada, 2019}. Citrate synthase (*cts-1*) and cyclin-dependent kinase 1 (*cdk-1*) were inhibited in these studies and halted *C. elegans* development, and both genes have orthologs in *S. carpocapsae*. Neutral lipids are formed from *sn*-glycerol-3-phosphate and are the major energy reserve in the closely related *S. feltiae* nematodes {Wright, 1997}. Fats are stored as lipid droplets in *C. elegans* dauer larvae intestines and serve as a starvation survival mechanism (Mak, 2012; O'Riordan, 1989). The previously mentioned glyoxylate bypass forms carbohydrates from fatty acids and has been implicated in extending the lifecycle of *C. elegans* {Edwards, 2013}, highlighting another role of this TCA vs. glyoxylate switching that could be happening later in the life cycle. Any indication that cholesterol is being synthesized from these intermediates can be attributed entirely to the insect's wheat germ diet, as the *X. nematophila*, *S. carpocapsae*, or *G. mellonella* cannot synthesize sterols but require them to grow {Dutky, 1967; Jing, 2020}.

Additionally, metabolites such as 2,3-dihydroxybenzoate that are not synthesized by *X. nematophila* or *S. carpocapsae* were found to increase over the infection, past insect death. *X. nematophila* does not encode the genes that convert 2,3-dihydroxybenzoate to the siderophore enterobactin, which bind iron to create the ferric enterobactin (FeEnt) complex {Raymond, 2003}. However, *X. nematophila* encodes FepB, a periplasmic enterobactin binding protein, as well as FepC, FepD, and FepG, which transport the FeEnt into the cell. This increased abundance of this compound suggests other *G. mellonella* microbiome members that survive infection synthesize a compound that is paramount in iron extraction and could contribute to the overall fitness of this symbiosis.

Metabolic analysis also revealed the significance in proline throughout the lifecycle. Insect hemolymph is rich in proline and is used as a main fuel source in some species of flying insects because of its ability to oxidize carbohydrates {Teulier, 2016; Goldstrohm, 2003}. Proline can be a signal molecule inducing secondary metabolite biosynthesis in *Xenorhabdus* species. Several known virulence factors and antibiotics are regulated via exogenously supplied proline to *Xenorhabdus* cultures {Crawford, 2010}. *Xenorhabdus* species may have evolved to use proline in insect hemolymph as a preferred amino acid source capable of enhancing the bacterium's virulence as well as protecting it from various stressors it meets in the insect body. Proline catabolism has also been implicated in promoting stress responses and modulating innate immunity in *C. elegans*, highlighting a possible mechanism by which *S. carpocapsae* survives reactive oxygen species produced by the insect, bacterium, or themselves {Tang, 2016}. Enhanced understanding of proline changes over time in the EPNB lifecycle highlights the multiple roles this amino acid is playing for both *Xenorhabdus* virulence and *Steinernema* protection and reproduction. Additional amino acids were found to exhibit similar concentration shifts over the lifecycle via the hierarchical clustering analysis. This machine learning technique can be improved with higher granularity of sample time points, which would strengthen the software developed for this study and allowing it to be used to study more complex and dynamic chemical environments.

We have shown how the parasitic EPNB infection shapes the insect host metabolism. The trophic hierarchy improved how we understand the parasites replicate in the host and highlights the importance of including microbes in these studies. Through rigorous metabolic pathway reconstruction and multivariate statistics, these results suggest each phase of the symbiosis can be characterized by stage-specific chemical signatures. Future targeted metabolomics experiments on EPNB symbioses should be developed to expand the specific

672 trends elucidated by this study. This work adds to a growing scientific foundation on how
673 symbioses, both mutualistic and parasitic, shape the chemical environments they inhabit.

674 **MATERIALS AND METHODS**

675 **Conventional nematode and aposymbiotic nematode production**

676 *S. carpocapsae* nematodes (All strain) were propagated through 5th instar larvae of insect *G.*
677 *mellonella* and using white trp and conventional IJs were collected by trapping in distilled water
678 at stored at room temperature for <1.5 months {McMullen, 2014}. To generate aposymbiotic IJs,
679 *X. nematophila* Δ*SR1* mutant were grown in Luria Broth (LB) media overnight at 30°C on cell
680 culture wheel and 600μL of overnight bacterial culture were spread onto each of 10mL of lipid
681 agar to grow into confluent lawn at 25°C for 48 hours. Conventional IJs were surface-sterilized,
682 seeded onto Δ*SR1* mutant lawn on lipid agar plates (5000 IJs per 10mL media), and incubated
683 at 25°C for 7 days in dark for nematode reproduction. Aposymbiotic IJs were collected by water-
684 trapping using distilled water and stored at room temperature in dark {McMullen, 2014}.

685 ***In vitro* controlled feeding experiment**

686 To collect bacteria sample feeding on terrestrial C3 plants and yeast-based media, *X.*
687 *nematophila* wildtype or Δ*SR1* mutant bacteria were grown in the dark yeast soy broth (0.5%
688 yeast extract, 3% tryptic soy broth, and 0.5% NaCl) modified from the bacterial growth media
689 from {Buecher and Popiel., 1989} at 30°C on cell culture wheel. Wildtype bacterial overnight
690 cultures (5mL per condition per biological replicate) were collected into microfuge tubes, spun
691 down at >5000RPM, and washed for three times using 1x PBS buffer by resuspending and
692 spinning down the bacterial pellets. Exactly 600μL of Δ*SR1* mutant were spread onto yeast-soy
693 lipid agar plates (0.5% yeast extract, 3% tryptic soy broth, 1.5% agar, 0.2% $MgCl_2$, 0.7% corn
694 syrup, 0.4% soy bean oil, supplemented with 40μg cholesterol at per liter of media) and
695 incubated for 48h at 25°C to grow into a confluent lawn. Bacterial lawns were washed off the

agar plate using 1x PBS, pelleted and washed as described above. Three individual tubes of bacterial culture were used per strain as three independent biological replicates.

To grow nematodes using a controlled diet, approximately 5000 conventional IJs were surface-sterilized and seeded onto bacterial lawn grown on yeast-soy lipid agar plate as described above. Three individual yeast-soy lipid agar plates were used as three biological replicates for each bacterial condition. Three days post seeding IJs, first generation reproductive stage of nematodes (adult males and females) were collected by flooding the bacterial lawn with 1x PBS buffer to resuspend the nematodes. The nematode suspension were collected in the glass cell culture tube and washed for three times by resuspending in 1x PBS buffer. Seven days post seeding the IJs, second generation IJ progenies were collected using distilled water traps and washed in water for three times (settle by gravity and resuspension).

In vivo feeding experiment and sample collection

To prepare insect controls, *G. mellonella* 5th instar larvae were injected with 10uL of either 1x PBS buffer, yeast-soy broth media, or nothing. Three insect larvae were prepared per condition as three biological replicates.

To collect nematodes directly fed on *Galleria* insect tissues, *S. carpocapsae* axenic eggs were extracted from adult female nematodes grown on yeast-soy lipid agar plates. Approximately 6000 axenic eggs were seeded to each of the *Galleria*-tissue agar plate (20% (w/v) frozen *G. mellonella* insects cleaned, blended and filtered; 0.5% (w/v) NaCl; and 1.5% (w/v) agar, supplemented with 50mg/L Kanamycin). Mixed-stages of nematodes were collected by flooding the *Galleria*-tissue agar with 1x PBS to resuspend the nematodes, then washed in 1x PBS and water for 3 times to separate nematodes from insect tissue debris.

To establish controlled feeding experiments *in vivo* for bacteria and nematodes, *X. nematophila* overnight cultures (in yeast-soy broth) were diluted in 1xPBS buffer, approximately 10^4 bacterial

720 cells were injected with or without aposymbiotic nematodes (100 IJs per insect). Insect cadaver
721 injected with bacteria only were directly lyophilized and used as insect-bacteria complex
722 controls (see methods below). Insects with bacteria and nematodes co-injection mixture were
723 used to collect IJ progenies by water-trapping, washing (3x in distilled water), and pelleting the
724 IJ samples. Three to five insects were used for each experimental condition as biological
725 replicates.

726 **Nematode lyophilization and trophic position analysis**

727 Nematodes from *G. mellonella* were collected by placing infected cadavers in modified White
728 traps in which nematodes migrate into distilled water. Trapped nematodes were transferred to
729 Falcon test tubes and allowed settle into a pellet at the bottom of the tube. Nematodes from
730 plate cultivations were harvested by rinsing with sterile distilled water, transferred to Falcon test
731 tubes, and allowed to settle. Samples of nematodes were stored in water at 10˚C no longer than
732 a few days until they were lyophilized. For lyophilization, water was decanted off of the sample
733 until only the undisturbed pellet remained at the bottom of the test tube. The top of the test tube
734 was covered with a Kimwipe held in place with a rubber band before lyophilization for >48 h in a
735 Labconco Freezone lyophilizer. During this time, pressures fell below 0.2 millibar, and
736 temperatures reached -50˚C. Once the samples had been thoroughly lyophilized, they were
737 removed from tubes using a laboratory spatula that was sterilized with ethanol and dried with
738 kimwipe after every use. Each individual sample was relocated into a sterile 1.5 ml microfuge
739 tube and stored at room temperature for 1-3 months until shipment to Hokkaido, Japan for
740 analysis.

741 Trophic position ($TP_{glu\text{-}phe}$) estimates were generated using the following equation:

742 $$TP = \frac{\delta^{15}N_{glu} - \delta^{15}N_{phe} + |\beta|}{\Delta_{glu-phe}} + \lambda$$

where $\delta^{15}N_{glu}$ represents the nitrogen isotopic ratio of glutamic acid, $\delta^{15}N_{phe}$ represents the nitrogen isotopic ratio of phenylalanine, β corrects for the difference in ^{15}N values between glutamic acid and phenylalanine within the primary producers of the food web (e.g. β~8.4‰ for C3 plants), $\Delta_{glu\text{-}phe}$ represents the net trophic discrimination between glutamic acid and phenylalanine, and λ represents the basal trophic level (=1) of the food web {Chikaraishi, 2014}. The trophic discrimination factor, $\Delta_{glu\text{-}phe}$ (referred to here as the $TDF_{glu\text{-}phe}$), represents the net intertrophic ^{15}N-discrimination between glutamic acid and phenylalanine. Significant differences between known and observed TP values were examined using univariate ANOVA and nonparametric tests (paired Wilcoxon signed rank tests where data were heteroscedastic). Distinguishing among TDF values was accomplished using paired t tests {Steffan, 2015}.

Metabolomics sample collection

As per normal infection protocols, 11 *G. mellonella* larvae (Grubco) were placed in the bottom of each of six 6 x 1.5 cm petri plates lined with 2 pieces of #1 filter paper. The filter paper was then inoculated with 1 ml of conventional *S. carpocapsae* IJ stage nematodes (carrying *X. nematophila* bacteria in their intestinal receptacle) to achieve a final average concentration of 10 IJ/µl. At each specified time point (see below), one *G. mellonella* was taken from each of plates 1-5. All insect samples were flash frozen using a dry ice-ethanol bath, and subsequently stored at -80ºC. The uninfected, Hour 1 post-infection and Hour 12 post-infection data points were taken of live *G. mellonella*. Since the *G. mellonella* were starting to succumb to the infection at Hour 24, one living and one dead insect was taken at this time point. At Day 7 post-infection, a water trap was set up to enable IJ emergence. At Day 12, the last of the *G. mellonella* from plates 1-5 was used, so insects representing the Day 16 time point were taken entirely from plate 6. Input *S. carpocapsae* IJ and *X. nematophila* symbionts were also collected from the lab stocks and sent for analysis, approximately 50 µl of settled IJ per sample, and a total of 4 samples were sent.

768 **Preparation for mass spectrometry**

769 For metabolite extraction, *G. mellonella* insects were equilibrated to -20˚C for ~1 h, 300 µl of
770 extraction solution (40:40:20 acetic acid, methanol, and water) was added, and insects were
771 ground using a pestle that fit snugly into the sample tube. All manipulations were performed in a
772 cold room and samples were processed in groups of 12. After grinding, to each tube an
773 additional 1000 µl of extraction solution was added and vortexed for 5-10 sec before being
774 placed at -20˚C for 20 min. Tubes were centrifuged at 16,200 x g for 5 min, and the supernatant
775 was decanted to a clean tube. To the original insect sample an additional 200 µl of extraction
776 solution was added, mixed with a pipette tip, vortexed for 5-10 sec, and incubated at -20˚C for
777 20 min. After pelleting the supernatant was combined with the first supernatant sample.
778 Samples were dried (Savant), resuspended, and randomized samples were analyzed
779 consecutively by mass spectrometry using an established 25 minute method (Lu, 2010).

780 **Metabolomics analysis**

781 An established untargeted metabolomics method utilizing ultra-high performance liquid
782 chromatography coupled to high resolution mass spectrometry (UHPLC-HRMS) (Thermo
783 Scientific, San Jose, CA, USA) was used to analyze water-soluble metabolites {Lu, 2010}. A
784 Synergi 2.6 µm Hydro RP column 100 Å, 100 mm x 2.1 mm (Phenomenex, Torrance, CA) and
785 an UltiMate 3000 pump (Thermo Fisher) were used to carry out the chromatographic
786 separations prior to full scan mass analysis by an Exactive Plus Orbitrap MS (Thermo Fisher).
787 HPLC grade solvents (Fisher Scientific, Hampton, NH, USA) were used. Chromatographic peak
788 areas for each detected metabolite were integrated using an open-source software package,
789 Metabolomic Analysis and Visualization Engine (MAVEN) {Clasquin, 2012; Melamud, 2010}.
790 Area under the curve (AUC) was used for further analyses.

791 **Statistical analysis**

PLS-DA plots were generated in MetaboAnalyst 4.0 on August 3rd, 2020. VIP scores were calculated for each component. When more than components are used to calculate the feature importance, the average of the VIP scores are used. The other importance measure is based on the weighted sum of PLS-regression. The weights are a function of the reduction of the sums of squares across the number of PLS components {Chong, 2020}. Samples were normalized before processing through MetaboAnalyst based on insect weight. Data was log transformed and pareto scaling was applied. Two-way ANOVA with multiple comparisons and Tukey post-hoc tests were completed by taking individual time point metabolite abundances and comparing their means to the uninfected insect model and each other. Student t-tests were performed by comparing uninfected samples to each time phase (early, middle, and late infection). Relevant metabolic pathways were identified in MetaboAnalyst's "Pathway Analysis" module using *Drosophila melanogaster*, *Caenorhabditis elegans*, and *Escherichia coli* as KEGG pathway libraries {Kanehisa, 2017}. Technical details for the hierarchical clustering analyses are available at: http://doi.org/10.5281/zenodo.3962081

Bacterial strains, plasmids, and culture conditions

File S2 lists strains used for this study with references where they were originally published. Unless specifically mentioned, *E. coli* were grown in LB broth or on LB plates at 37°C; *X. nematophila* were grown in LB broth or on LB plates supplemented with 0.1% pyruvate at 30°C and kept in dark. Where appropriate, the following antibiotic concentrations were used: ampicillin, 150 µg/ml for *E. coli* and 50 µg/ml for *X. nematophila*; chloramphenicol, 30 µg/ml; erythromycin, 200 µg/ml; kanamycin, 50 µg/ml and streptomycin, 25 µg/ml. *E. coli* donor strain S17 (λpir) or Δ*asd* strain BW29427 was used to conjugate plasmids into *X. nematophila*.

Microarray experiment and data analysis

Bacteria cultures were grown overnight in 3 ml of LB supplemented with 0.1% pyruvate and appropriate antibiotics in culture tubes at 30°C on roller, subcultured 1:100 into 30 ml of LB supplemented with 0.1% pyruvate and 50 g/ml ampicillin in 125 ml glass flasks and grown for 12 hours to early stationary phase (OD 2-2.1) at 30°C at 150 rpm on shaker. 1 ml of each culture was used to extract total RNA using Qiagen RNeasy Mini Kit, and on-column DNA digestion was performed using Qiagen RNase-Free DNase Set according to manufacturer's protocol (Qiagen, Valencia, CA). The RNA purity was tested by measuring 260 nm/280 nm and 260 nm/230 nm ratios in TE buffer and the values should be over 1.8. RNA integrity was verified by running 2 g of RNA samples on 1% denaturing agarose gel. The samples were then submitted to Roche NimbleGen for processing and microarray analysis. Gene signals for *lrhA*, *lrp*, and secondary form *X. nematophila* were compared to HGB800 using a 2-fold change average signal strength cutoff. The *rpoS* mutant was compared to HGB007 using the same significance cutoff. Genes were annotated via the Magnifying Genomes (MaGe) microbial genome annotation system {Vallenet, 2006}, the STRING database {Szklarczyk, 2019}, as well as through BlastKOALA {Kanehisa, 2016}.

ACKNOWLEDGEMENTS

This work was supported by a grant to H.G.-B. from the National Science Foundation (IOS-1353674) and by funds from the University of Tennessee-Knoxville. M.C. was supported by a UW-Madison Louis and Elsa Thomsen Wisconsin Distinguished Graduate Fellowship and a Department of Bacteriology Michael Foster Predoctoral Fellowship. We thank Terra Mauer for her help in insect rearing and providing the *G. mellonella* image used for Figure 1. We thank Xiaojun Lu for preprocessing the microarray data. We thank Jordan Rogerson for processing the metabolomics samples prior analysis.

REFERENCES

1. **Abdelhamed H., Ramachandran R., Narayanan L., Ozdemir O., Cooper A., Olivier A. K., Karsi A., Lawrence M. L.** (2020). Contributions of a LysR Transcriptional Regulator to *Listeria monocytogenes* Virulence and Identification of Its Regulons. *J Bacteriol*, 202(10). doi:10.1128/JB.00087-20
2. **Alaimo J. T., Davis S. J., Song S. S., Burnette C. R., Grotewiel M., Shelton K. L., Pierce-Shimomura J. T., Davies A. G., Bettinger J. C.** (2012). Ethanol metabolism and osmolarity modify behavioral responses to ethanol in *C. elegans*. *Alcohol Clin Exp Res*, 36(11), 1840-1850. doi:10.1111/j.1530-0277.2012.01799.x
3. **Baliadi Y, Yoshiga T, Kondo E.** (2004) Infectivity and post-infection development of infective juveniles originating via endotokia matricida in entomopathogenic nematodes. *Applied Entomology and Zoology*;39:61–69.
4. **Budnick J. A., Sheehan L. M., Ginder M. J., Failor K. C., Perkowski J. M., Pinto J. F., Kohl K. A., Kang L., Michalak P., Luo L., Heindl J. E., Caswell C. C.** (2020). A central role for the transcriptional regulator VtlR in small RNA-mediated gene regulation in *Agrobacterium tumefaciens*. *Sci Rep*, 10(1), 14968. doi:10.1038/s41598-020-72117-0
5. **Buecher E. J., Popiel I.** (1989). Liquid Culture of the Entomogenous Nematode *Steinernema feltiae* with Its Bacterial Symbiont. *J Nematol*, 21(4), 500-504. Retrieved from https://www.ncbi.nlm.nih.gov/pubmed/19287644
6. **Blumer C., Kleefeld A., Lehnen D., Heintz M., Dobrindt U., Nagy G., Michaelis K., Emödy L., Polen T., Rachel R., Wendisch V. F., Unden G**. (2005). Regulation of type 1 fimbriae synthesis and biofilm formation by the transcriptional regulator LrhA of *Escherichia coli*. *Microbiology,* 151(Pt 10), 3287-3298. doi:10.1099/mic.0.28098-0
7. **Cambon M. C., Lafont P., Frayssinet M., Lanois A., Ogier J. C., Pages S., Parthuisot N., Ferdy J. B., Gaudriault S**. (2020). Bacterial community profile after the

lethal infection of *Steinernema-Xenorhabdus* pairs into soil-reared *Tenebrio molitor* larvae. *FEMS Microbiol Ecol,* 96(2). doi:10.1093/femsec/fiaa009

8. **Camilli A., Bassler B. L.** (2006). Bacterial small-molecule signaling pathways. *Science,* 311(5764), 1113-1116. doi:10.1126/science.1121357
9. **Cao M., Goodrich-Blair H.** (2020). *Xenorhabdus nematophila* bacteria shift from mutualistic to virulent Lrp-dependent phenotypes within the receptacles of *Steinernema carpocapsae* insect-infective stage nematodes. *Environ Microbiol*, 22(12), 5433-5449. doi:10.1111/1462-2920.15286
10. **Chaston J., Douglas A. E.** (2012). Making the most of "omics" for symbiosis research. *Biol Bull*, 223(1), 21-29. doi:10.1086/BBLv223n1p21
11. **Chaston J. M., Suen G., Tucker S. L., Andersen A. W., Bhasin A., Bode E., Bode H. B., Brachmann A. O., Cowles C. E., Cowles K. N., Darby C., de Léon L., Drace K., Du Z., Givaudan A., Herbert Tran E. E., Jewell K. A., Knack J. J., Krasomil-Osterfeld K. C., Kukor R., Lanois A., Latreille P., Leimgruber N. K., Lipke C. M., Liu R., Lu X., Martens E. C., Marri P. R., Médigue C., Menard M. L., Miller N. M., Morales-Soto N., Norton S., Ogier J. C., Orchard S. S., Park D., Park Y., Qurollo B. A., Sugar D. R., Richards G. R., Rouy Z., Slominski B., Slominski K., Snyder H., Tjaden B. C., van der Hoeven R., Welch R. D., Wheeler C., Xiang B., Barbazuk B., Gaudriault S., Goodner B., Slater S. C, Forst S., Goldman B. S., Goodrich-Blair H.** (2011). The entomopathogenic bacterial endosymbionts *Xenorhabdus* and *Photorhabdus*: convergent lifestyles from divergent genomes. *PLoS One*. 6(11):e27909. doi: 10.1371/journal.pone.0027909. PMID: 22125637; PMCID: PMC3220699.
12. **Chikaraishi Y., Kashiyama Y., Ogawa N. O., Kitazato H., Ohkouchi N.** (2007). Biosynthetic and metabolic controls of nitrogen isotopic composition of amino acids in marine macroalgae and gastropods: implications for aquatic food web studies. Mar. *Ecol. Prog*. Ser. 342: 85– 90.

13. **Chikaraishi Y., Ogawa N. O., Kashiyama Y., Takano Y., Suga H., Tomitani A., Ohkouchi N.** (2009). Determination of aquatic food-web structure based on compound-specific nitrogen isotopic composition of amino acids. *Limnol. Oceanogr. Methods* 7: 740– 750.

14. **Chikaraishi Y., Ogawa N.O., Doi H., Ohkouchi N.** (2011) $^{15}N/^{14}N$ ratios of amino acids as a tool for studying terrestrial food webs: a case study of terrestrial insects (bees, wasps, and hornets). *Ecol. Res*.;26:835–844.

15. **Chikaraishi Y., Steffan S. A., Ogawa N. O., Ishikawa N. F., Sasaki Y., Tsuchiya M., Ohkouchi N.** (2014). High-resolution food webs based on nitrogen isotopic composition of amino acids. *Ecol Evol,* 4(12), 2423-2449. doi:10.1002/ece3.1103

16. **Chong J., Xia J.** (2020). Using MetaboAnalyst 4.0 for Metabolomics Data Analysis, Interpretation, and Integration with Other Omics Data. *Methods Mol Biol, 2104*, 337-360. doi:10.1007/978-1-0716-0239-3_17

17. **Chung J. C., Rzhepishevska O., Ramstedt M., Welch M. (**2013). Type III secretion system expression in oxygen-limited *Pseudomonas aeruginosa* cultures is stimulated by isocitrate lyase activity. *Open Biol*, 3(1), 120131. doi:10.1098/rsob.120131

18. **Ciche T. A., Blackburn M., Carney J. R., Ensign J. C.** (2003). Photobactin: a catechol siderophore produced by *Photorhabdus luminescens*, an entomopathogen mutually associated with *Heterorhabditis bacteriophora* NC1 nematodes. *Appl Environ Microbiol*, 69(8), 4706-4713. doi:10.1128/aem.69.8.4706-4713.2003

19. **Clark K. D., Lu Z., Strand M. R.** (2010). Regulation of melanization by glutathione in the moth *Pseudoplusia includens*. *Insect Biochem Mol Biol*, 40(6), 460-467. doi:10.1016/j.ibmb.2010.04.005

20. **Clasquin M. F., Melamud E., Rabinowitz J. D.** (2012). LC-MS data processing with MAVEN: a metabolomic analysis and visualization engine. *Curr Protoc Bioinformatics*, Chapter 14, Unit14 11. doi:10.1002/0471250953.bi1411s37

21. **Cobb N. A.** (1914). Nematodes and their relationships. *Yearbook United States Department Agriculture*, 457-490.

22. **Colinvaux P. A., Barnett B. D.** (1979). Lindeman and the Ecological Efficiency of Wolves. *Am. Nat*.; 114: 707-718

23. **Cowles C. E., Goodrich-Blair H.** (2006). *nilR* is necessary for co-ordinate repression of *Xenorhabdus nematophila* mutualism genes. *Molecular Microbiology*; 62:760-771.

24. **Cowles C. E., Goodrich-Blair H.** (2008). The *Xenorhabdus nematophila nilABC* genes confer the ability of *Xenorhabdus* spp. to colonize *Steinernema carpocapsae* nematodes. J Bacteriol, 190(12), 4121-4128. doi:10.1128/JB.00123-08

25. **Cowles K. N., Cowles C. E., Richards G. R., Martens E. C., Goodrich-Blair H. (**2007). The global regulator Lrp contributes to mutualism, pathogenesis and phenotypic variation in the bacterium *Xenorhabdus nematophila*. *Cell Microbiol,* 9(5), 1311-1323. doi:10.1111/j.1462-5822.2006.00873.x

26. **Crawford J. M., Kontnik R., Clardy J. (**2010). Regulating alternative lifestyles in entomopathogenic bacteria. *Curr Biol,* 20(1), 69-74. doi:10.1016/j.cub.2009.10.059

27. **da Silva W. J., Pilz-Junior H. L., Heermann R., da Silva O. S.** (2020). The great potential of entomopathogenic bacteria *Xenorhabdus* and *Photorhabdus* for mosquito control: a review. *Parasit Vectors*, 13(1), 376. doi:10.1186/s13071-020-04236-6

28. **De Mets F., Van Melderen L., Gottesman S.** (2019). Regulation of acetate metabolism and coordination with the TCA cycle via a processed small RNA. *Proc Natl Acad Sci U S A*, 116(3), 1043-1052. doi:10.1073/pnas.1815288116

29. **Dearth S. P., Castro H. F., Venice F., Tague E. D., Novero M., Bonfante P., Campagna S. R.** (2018). Metabolome changes are induced in the arbuscular mycorrhizal fungus *Gigaspora margarita* by germination and by its bacterial endosymbiont. *Mycorrhiza*, 28(5-6), 421-433. doi:10.1007/s00572-018-0838-8

30. **Di Martino M. L., Campilongo R., Casalino M., Micheli G., Colonna B., Prosseda G.** (2013). Polyamines: emerging players in bacteria-host interactions. *Int J Med Microbiol,* 303(8), 484-491. doi:10.1016/j.ijmm.2013.06.008

31. **Doberenz C., Zorn M., Falke D., Nannemann D., Hunger D., Beyer L., Ihling C. H., Meiler J., Sinz A., Sawers R. G.** (2014). Pyruvate formate-lyase interacts directly with the formate channel FocA to regulate formate translocation. *J Mol Biol,* 426(15), 2827-2839. doi:10.1016/j.jmb.2014.05.023

32. **Dong Y., Brewer G. J.** (2019). Global Metabolic Shifts in Age and Alzheimer's Disease Mouse Brains Pivot at NAD+/NADH Redox Sites. *J Alzheimers Dis*, 71(1), 119-140. doi:10.3233/JAD-190408

33. **Dutky S. R., Robbins W. F., Thompson J. V.** (1967). The demonstration of sterols as requirements for the growth, development and reproduction of the DD- 136 nematode. *Nematologica*;13:140.

34. **Edwards C. B., Copes N., Brito A. G., Canfield J., Bradshaw P. C.** (2013). Malate and fumarate extend lifespan in *Caenorhabditis elegans*. *PLoS One,* 8(3), e58345. doi:10.1371/journal.pone.0058345

35. **Elton C. S.** (1927). Animal Ecology. Sidgwick & Jackson, London.

36. **Gibson K. E., Silhavy T. J.** (1999). The LysR homolog LrhA promotes RpoS degradation by modulating activity of the response regulator *sprE*. *J Bacteriol,* 181(2), 563-571. Retrieved from https://www.ncbi.nlm.nih.gov/pubmed/9882671

37. **Givaudan A., Baghdiguian S., Lanois A., Boemare N.** (1995). Swarming and Swimming Changes Concomitant with Phase Variation in *Xenorhabdus nematophilus*. *Appl Environ Microbiol*, 61(4), 1408-1413. doi:10.1128/AEM.61.4.1408-1413.1995

38. **Givaudan A., Lanois A.** (2000). *flhDC*, the flagellar master operon of *Xenorhabdus nematophilus*: requirement for motility, lipolysis, extracellular hemolysis, and full virulence in insects. *J Bacteriol,* 182(1), 107-115. doi:10.1128/jb.182.1.107-115.2000

967 39. **Goldstrohm D. A., Pennington J. E., Wells M. A.** (2003). The role of hemolymph
968 proline as a nitrogen sink during blood meal digestion by the mosquito *Aedes aegypti*. *J*
969 *Insect Physiol,* 49(2), 115-121. doi:10.1016/s0022-1910(02)00267-6
970 40. **Grabau Z. J., Mauldin M. D., Habteweld A., Carter E. T.** (2020). Nematicide efficacy at
971 managing *Meloidogyne arenaria* and non-target effects on free-living nematodes in
972 peanut production. *J Nematol, 52*, 1-10. doi:10.21307/jofnem-2020-028
973 41. **Hada K., Hirota K., Inanobe A., Kako K., Miyata M., Araoi S., Matsumoto M., Ohta**
974 **R., Arisawa M., Daitoku H., Hanada T., Fukamizu A**. (2019). Tricarboxylic acid cycle
975 activity suppresses acetylation of mitochondrial proteins during early embryonic
976 development in *Caenorhabditis elegans*. *J Biol Chem,* 294(9), 3091-3099.
977 doi:10.1074/jbc.RA118.004726
978 42. **Harris S. J., Shih Y. L., Bentley S. D., Salmond G. P.** (1998). The *hexA* gene of
979 *Erwinia carotovora* encodes a LysR homologue and regulates motility and the
980 expression of multiple virulence determinants. *Mol Microbiol, 28*(4), 705-717.
981 doi:10.1046/j.1365-2958.1998.00825.x
982 43. **Henikoff S., Haughn G. W., Calvo J. M., Wallace J. C.** (1988). A large family of
983 bacterial activator proteins. *Proc Natl Acad Sci U S A*, 85(18), 6602-6606.
984 doi:10.1073/pnas.85.18.6602
985 44. **Herbert E. E., Goodrich-Blair H.** (2007). Friend and foe: the two faces of *Xenorhabdus*
986 *nematophila*. *Nat Rev Microbiol,* 5(8), 634-646. doi:10.1038/nrmicro1706
987 45. **Heroven A. K., Dersch P.** (2006). RovM, a novel LysR-type regulator of the virulence
988 activator gene *rovA*, controls cell invasion, virulence and motility of *Yersinia*
989 *pseudotuberculosis*. *Mol Microbiol,* 62(5), 1469-1483. doi:10.1111/j.1365-
990 2958.2006.05458.x

46. **Hussa E. A., Casanova-Torres A. M., Goodrich-Blair H. (**2015). The global transcription factor Lrp controls virulence modulation in *Xenorhabdus nematophila*. *J Bacteriol*; 197:3015-3025.

47. **Joyce S. A., Clarke D. J.** (2003). A *hexA* homologue from *Photorhabdus* regulates pathogenicity, symbiosis and phenotypic variation. *Mol Microbiol,* 47(5), 1445-1457. doi:10.1046/j.1365-2958.2003.03389.x

48. **Kanehisa M., Sato Y., Morishima K.** (2016) BlastKOALA and GhostKOALA: KEGG tools for functional characterization of genome and metagenome sequences. *J. Mol. Biol*. 428, 726-731.

49. **Kanehisa M., Furumichi M., Tanabe M., Sato Y., Morishima K.** (2017). KEGG: new perspectives on genomes, pathways, diseases and drugs. *Nucleic Acids Res*, 45(D1), D353-D361. doi:10.1093/nar/gkw1092

50. **Katsyuba E., Mottis A., Zietak M., De Franco F., van der Velpen V., Gariani K., Ryu D., Cialabrini L., Matilainen O., Liscio P., Giacchè N., Stokar-Regenscheit N., Legouis D., de Seigneux S., Ivanisevic J., Raffaelli N., Schoonjans K., Pellicciari R., Auwerx J.** (2018). De novo NAD+ synthesis enhances mitochondrial function and improves health. *Nature*. 563(7731):354-359. doi: 10.1038/s41586-018-0645-6. PMID: 30356218; PMCID: PMC6448761.

51. **Killiny N.** (2018). Generous hosts: Why the larvae of greater wax moth, *Galleria mellonella* is a perfect infectious host model? *Virulence*, 9(1), 860-865. doi:10.1080/21505594.2018.1454172

52. **Lacey L. A., Georgis, R.** (2012). Entomopathogenic nematodes for control of insect pests above and below ground with comments on commercial production. *J Nematol,* 44(2), 218-225. Retrieved from https://www.ncbi.nlm.nih.gov/pubmed/23482993

53. **Latham J. A., Chen D., Allen K. N., Dunaway-Mariano D.** (2014). Divergence of substrate specificity and function in the *Escherichia coli* hotdog-fold thioesterase paralogs YdiI and YbdB. *Biochemistry*, 53(29), 4775-4787. doi:10.1021/bi500333m

54. **Lehnen D., Blumer C., Polen T., Wackwitz B., Wendisch V. F., Unden G.** (2002). LrhA as a new transcriptional key regulator of flagella, motility and chemotaxis genes in *Escherichia coli*. *Mol Microbiol,* 45(2), 521-532. doi:10.1046/j.1365-2958.2002.03032.x

55. **Lee Y., Jeong H., Park K. H., Kim K. W.** (2020). Effects of NAD(+) in *Caenorhabditis elegans* Models of Neuronal Damage. Biomolecules, 10(7). doi:10.3390/biom10070993

56. **Lindeman R.L.** (1942). The trophic-dynamic aspect of ecology. *Ecology*, 23, pp. 399-417

57. **Javal M., Terblanche J. S., Conlong D. E., Malan, A. P.** (2019). First Screening of Entomopathogenic Nematodes and Fungus as Biocontrol Agents against an Emerging Pest of Sugarcane, *Cacosceles newmannii* (Coleoptera: Cerambycidae). *Insects*, 10(4). doi:10.3390/insects10040117

58. **Jing X., Behmer S. T.** (2020). Insect Sterol Nutrition: Physiological Mechanisms, Ecology, and Applications. *Annu Rev Entomol*, 65, 251-271. doi:10.1146/annurev-ento-011019-025017

59. **Lu W., Clasquin M. F., Melamud E., Amador-Noguez D., Caudy A. A., Rabinowitz J. D.** (2010). Metabolomic analysis via reversed-phase ion-pairing liquid chromatography coupled to a stand alone orbitrap mass spectrometer. *Anal Chem*, 82(8), 3212-3221. doi:10.1021/ac902837x

60. **Lu X., Goodrich-Blair H., Tjaden B.** (2011). Assessing computational tools for the discovery of small RNA genes in bacteria. *RNA*; 17:1635-1647.

61. **Lu X.** (2012). Examining Pathogenic and Mutualistic Regulatory Networks in the Bacterium *Xenorhabdus nematophila*. Ph.D. thesis, UW-Madison

62. **Maddocks S. E., Oyston P. C. F.** (2008). Structure and function of the LysR-type transcriptional regulator (LTTR) family proteins. *Microbiology*, 154(Pt 12), 3609-3623. doi:10.1099/mic.0.2008/022772-0

63. **Mak H. Y.** (2012) Lipid droplets as fat storage organelles in *Caenorhabditis elegans*: thematic review series: lipid droplet synthesis and metabolism: from yeast to man. *J Lipid Res*.;53(1):28–33.

64. **Maloy S. R., Nunn W. D.** (1982). Genetic regulation of the glyoxylate shunt in *Escherichia coli* K-12. *J Bacteriol*, 149(1), 173-180. Retrieved from https://www.ncbi.nlm.nih.gov/pubmed/7033207

65. **Margulis L.** (1981). *Symbiosis in cell evolution: life and its environment on the early Earth*. San Francisco: W. H. Freeman.

66. **Martens E. C., Vivas E. I., Heungens K., Cowles C. E., Goodrich-Blair H**. (2004) Investigating mutualism between entomopathogenic bacteria and nematodes. *Nematol. Monographs Persp.* 2, 447–462

67. **Martens E. C., Russell F. M., Goodrich-Blair H.** (2005). Analysis of *Xenorhabdus nematophila* metabolic mutants yields insight into stages of *Steinernema carpocapsae* nematode intestinal colonization. *Mol Microbiol, 58*(1), 28-45. doi:10.1111/j.1365-2958.2005.04742.x

68. **Martino G. P., Perez C. E., Magni C., Blancato V. S.** (2018). Implications of the expression of *Enterococcus faecalis* citrate fermentation genes during infection. *PLoS One,* 13(10), e0205787. doi:10.1371/journal.pone.0205787

69. **May J. M., Qu Z. C., Meredith M. E.** (2012). Mechanisms of ascorbic acid stimulation of norepinephrine synthesis in neuronal cells. *Biochem Biophys Res Commun*, 426(1), 148-152. doi:10.1016/j.bbrc.2012.08.054

70. **McMullen J. G. 2nd, Stock S. P**. (2014). *In vivo* and *in vitro* rearing of entomopathogenic nematodes (*Steinernematidae* and *Heterorhabditidae*). *J Vis Exp,* (91), 52096. doi:10.3791/52096

71. **Melamud E., Vastag L., Rabinowitz J. D.** (2010). Metabolomic analysis and visualization engine for LC-MS data. *Anal Chem*, 82(23), 9818-9826. doi:10.1021/ac1021166

72. **O'Riordan V. B., Burnell A. M.** (1989) Intermediary metabolism in the dauer larva of the nematode *Caenorhabditis elegans*— 1. Glycolysis, gluconeogenesis, oxidative phosphorylation and the tricarboxylic acid cycle. *Comp Biochem Physiol B*.;92(2):233–8.

73. **Ohkouchi N., Chikaraishi Y., Close H. G., Fry B., Larsen T., Madigan D. J., McCarthy M. D., McMahon K. W., Nagata T., Naito Y. I., Ogawa N. O., Popp B. N., Steffan S., Takano Y., Tayasu I., Wyatt A. S. J., Yamaguchi Y. T., Yokoyama Y.** (2017). Advances in the application of amino acid nitrogen isotopic analysis in ecological and biogeochemical studies. *Organic Geochemistry*, Volume 113, 150-174. https://doi.org/10.1016/j.orggeochem.2017.07.009.

74. **Orchard S. S., Goodrich-Blair H.** (2005). Pyrimidine nucleoside salvage confers an advantage to *Xenorhabdus nematophila* in its host interactions. *Appl Environ Microbiol,* 71(10), 6254-6259. doi:10.1128/AEM.71.10.6254-6259.2005

75. **Park S. J., Tseng C. P., Gunsalus R. P.** (1995). Regulation of succinate dehydrogenase (*sdhCDAB*) operon expression in *Escherichia coli* in response to carbon supply and anaerobiosis: role of ArcA and Fnr. *Mol Microbiol,* 15(3), 473-482. doi:10.1111/j.1365-2958.1995.tb02261.x

76. **Perinbam K., Chacko J. V., Kannan A., Digman M. A., Siryaporn A.** (2020). A Shift in Central Metabolism Accompanies Virulence Activation in *Pseudomonas aeruginosa*. *mBio,* 11(2). doi:10.1128/mBio.02730-18

77. **Peterson C. N., Carabetta V. J., Chowdhury T., Silhavy T. J.** (2006). LrhA regulates *rpoS* translation in response to the Rcs phosphorelay system in *Escherichia coli*. *J Bacteriol,* 188(9), 3175-3181. doi:10.1128/JB.188.9.3175-3181.2006

78. **Phelan V. V., Moree W. J., Aguilar J., Cornett D. S., Koumoutsi A., Noble S. M., Pogliano K., Guerrero C. A., Dorrestein P. C.** (2014). Impact of a transposon insertion in phzF2 on the specialized metabolite production and interkingdom interactions of *Pseudomonas aeruginosa*. *J Bacteriol*, 196(9), 1683-1693. doi:10.1128/JB.01258-13

79. **Rahman M. M., Rosu S., Joseph-Strauss D., Cohen-Fix O.** (2014). Down-regulation of tricarboxylic acid (TCA) cycle genes blocks progression through the first mitotic division in *Caenorhabditis elegans* embryos. *Proc Natl Acad Sci U S A,* 111(7), 2602-2607. doi:10.1073/pnas.1311635111

80. **Ramarao N., Nielsen-Leroux C., Lereclus D.** (2012). The insect *Galleria mellonella* as a powerful infection model to investigate bacterial pathogenesis. *J Vis Exp*(70), e4392. doi:10.3791/4392

81. **Raymond K. N., Dertz E. A., Kim S. S.** (2003). Enterobactin: an archetype for microbial iron transport. *Proc Natl Acad Sci U S A*, 100(7), 3584-3588. doi:10.1073/pnas.0630018100

82. **Ren J., Sang Y., Lu J., Yao Y. F.** (2017). Protein Acetylation and Its Role in Bacterial Virulence. *Trends Microbiol*, 25(9), 768-779. doi:10.1016/j.tim.2017.04.001

83. **Richards G. R., Goodrich-Blair H.** (2009). Masters of conquest and pillage: *Xenorhabdus nematophila* global regulators control transitions from virulence to nutrient acquisition. *Cell Microbiol, 11*(7), 1025-1033. doi:10.1111/j.1462-5822.2009.01322.x

84. **Richards G. R., Herbert E. E., Park Y., Goodrich-Blair, H. (**2008). *Xenorhabdus nematophila lrhA* is necessary for motility, lipase activity, toxin expression, and virulence in *Manduca sexta* insects. *J Bacteriol, 190*(14), 4870-4879. doi:10.1128/JB.00358-08

85. **Rougon-Cardoso A., Flores-Ponce M., Ramos-Aboites H. E., Martínez-Guerrero C. E., Hao Y. J., Cunha L., Rodríguez-Martínez J. A., Ovando-Vázquez C., Bermúdez-Barrientos J. R., Abreu-Goodger C., Chavarría-Hernández N., Simões N., Montiel R.** (2016). The genome, transcriptome, and proteome of the nematode *Steinernema carpocapsae*: evolutionary signatures of a pathogenic lifestyle. *Sci Rep*, 6, 37536. doi:10.1038/srep37536

86. **Shah P., Swiatlo E.** (2008). A multifaceted role for polyamines in bacterial pathogens. *Mol Microbiol*, 68(1), 4-16. doi:10.1111/j.1365-2958.2008.06126.x

87. **Shi Y., Wang H., Yan Y., Cao H., Liu X., Lin F., Lu J**. (2018). Glycerol-3-Phosphate Shuttle Is Involved in Development and Virulence in the Rice Blast Fungus *Pyricularia oryzae*. *Front Plant Sci,* 9, 687. doi:10.3389/fpls.2018.00687

88. **Stahlschmidt Z., Acker M., Kovalko I., Adamo S.** (2015). The double-edged sword of immune defence and damage control: Do food availability and immune challenge alter the balance? *Functional Ecology.* 29. 10.1111/1365-2435.12454.

89. **Steffan S. A., Chikaraishi Y., Horton D. R., Ohkouchi N., Singleton M. E., Miliczky E., Hogg D. B., Jones V. P.** (2013). Trophic hierarchies illuminated via amino acid isotopic analysis. *PLoS One*, 8(9), e76152. doi:10.1371/journal.pone.0076152

90. **Steffan S. A., Chikaraishi Y., Currie C. R., Horn H., Gaines-Day H. R., Pauli J. N., Zalapa J. E., Ohkouchi N.** (2015). Microbes are trophic analogs of animals. *Proc Natl Acad Sci U S A,* 112(49), 15119-15124. doi:10.1073/pnas.1508782112

91. **Steffan S. A., Chikaraishi Y., Dharampal P. S., Pauli J. N., Guedot C., Ohkouchi N.** (2017). Unpacking brown food-webs: Animal trophic identity reflects rampant microbivory. *Ecol Evol*, 7(10), 3532-3541. doi:10.1002/ece3.2951

92. **Steffan S. A., Dharampal P. S.** (2019). Undead food-webs: Integrating microbes into the food-chain. *Food Webs*, 18, e00111. https://doi.org/10.1016/j.fooweb.2018.e00111

93. **Stock S. P.** (2019). Partners in crime: symbiont-assisted resource acquisition in *Steinernema* entomopathogenic nematodes. *Curr Opin Insect Sci*, 32, 22-27. doi:10.1016/j.cois.2018.10.006

94. **Szklarczyk D., Gable A. L., Lyon D., Junge A., Wyder S., Huerta-Cepas J., Simonovic M., Doncheva N. T., Morris J. H., Bork P., Jensin L. J., Mering C. V.** (2019). STRING v11: protein-protein association networks with increased coverage, supporting functional discovery in genome-wide experimental datasets. *Nucleic Acids Res*, 47(D1), D607-D613. doi:10.1093/nar/gky1131

95. **Takizawa Y., Takano Y., Choi B., Dharampal P. S., Steffan S. A., Ogawa N. O., Ohkouchi N., Chikaraishi Y.** (2020). A new insight into isotopic fractionation associated with decarboxylation in organisms: implications for amino acid isotope approaches in biogeoscience. *Prog Earth Planet Sci* 7, 50. https://doi.org/10.1186/s40645-020-00364-w

96. **Tang H., Pang S.** (2016). Proline Catabolism Modulates Innate Immunity in *Caenorhabditis elegans*. *Cell Rep,* 17(11), 2837-2844. doi:10.1016/j.celrep.2016.11.038

97. **Tang J.** (2011). Microbial metabolomics. *Curr Genomics, 12*(6), 391-403. doi:10.2174/138920211797248619

98. **Teulier L., Weber J. M., Crevier J., Darveau C. A. (**2016). Proline as a fuel for insect flight: enhancing carbohydrate oxidation in hymenopterans. *Proc Biol Sci,* 283(1834). doi:10.1098/rspb.2016.0333

99. **Tsai C. J., Loh J. M., Proft T.** (2016). *Galleria mellonella* infection models for the study of bacterial diseases and for antimicrobial drug testing. *Virulence,* 7(3), 214-229. doi:10.1080/21505594.2015.1135289

100. **Vallenet D., Labarre L., Rouy Z., Barbe V., Bocs S., Cruveiller S., Lajus A., Pascal G., Scarpelli C., Médigue C.** (2006). MaGe: a microbial genome annotation system supported by synteny results. *Nucleic Acids Res*, 34(1), 53-65. doi:10.1093/nar/gkj406

101. **Vivas E.I., Goodrich-Blair H.** (2001) *Xenorhabdus nematophilus* as a model for host-bacterium interactions: rpoS is necessary for mutualism with nematodes. *Journal of Bacteriology*; 183:4687-4693.

102. **Volgyi A, Fodor A, Szentirmai A, Forst S.** (1998). Phase Variation in *Xenorhabdus nematophilus*. *Appl Environ Microbiol*.;64(4):1188-93. doi: 10.1128/AEM.64.4.1188-1193. PMID: 16349534

103. **Wang J., Dong Y., Zhou T., Liu X., Deng Y., Wang C., Lee J., Zhang L. H.** (2013) *Pseudomonas aeruginosa* cytotoxicity is attenuated at high cell density and associated with the accumulation of phenylacetic acid. *PLoS One*.;8(3):e60187. doi:10.1371/journal.pone.0060187

104. **Watford M.** (2008). Glutamine metabolism and function in relation to proline synthesis and the safety of glutamine and proline supplementation. *J Nutr,* 138(10), 2003S-2007S. doi:10.1093/jn/138.10.2003S

105. **Worthington R. J., Richards J. J., Melander C.** (2012). Small molecule control of bacterial biofilms. *Org Biomol Chem*, 10(37), 7457-7474. doi:10.1039/c2ob25835h

106. **Yokoyama K., Ishijima S. A., Clowney L., Koike H., Aramaki H., Tanaka C., Makino K., Suzuki M.** (2006). Feast/famine regulatory proteins (FFRPs): *Escherichia coli* Lrp, AsnC and related archaeal transcription factors. *FEMS Microbiol Rev*, 30(1), 89-108. doi:10.1111/j.1574-6976.2005.00005.x

107. **You D., Yao L. L., Huang D., Escalante-Semerena J. C., Ye B. C.** (2014). Acetyl coenzyme A synthetase is acetylated on multiple lysine residues by a protein acetyltransferase with a single Gcn5-type N-acetyltransferase (GNAT) domain in *Saccharopolyspora erythraea*. *J Bacteriol.*;196(17):3169-3178. doi:10.1128/JB.01961-14

108. **Zečić A., Dhondt I., Braeckman B.P.** (2019). The nutritional requirements of *Caenorhabditis elegans*. *Genes Nutr* 14, 15 (2019). https://doi.org/10.1186/s12263-019-0637-7

109. **Zelcbuch L., Lindner S. N., Zegman Y., Vainberg Slutskin I., Antonovsky N., Gleizer S., Milo R., Bar-Even A.** (2016). Pyruvate Formate-Lyase Enables Efficient Growth of *Escherichia coli* on Acetate and Formate. *Biochemistry*, 55(17), 2423-2426. doi:10.1021/acs.biochem.6b00184

110. **Zheng R., Feng X., Wei X., Pan X., Liu C., Song R., Jin Y., Bai F., Jin S., Wu Wu., Cheng Z.** (2018). PutA Is Required for Virulence and Regulated by PruR in *Pseudomonas aeruginosa*. *Front Microbiol,* 9, 548. doi:10.3389/fmicb.2018.00548

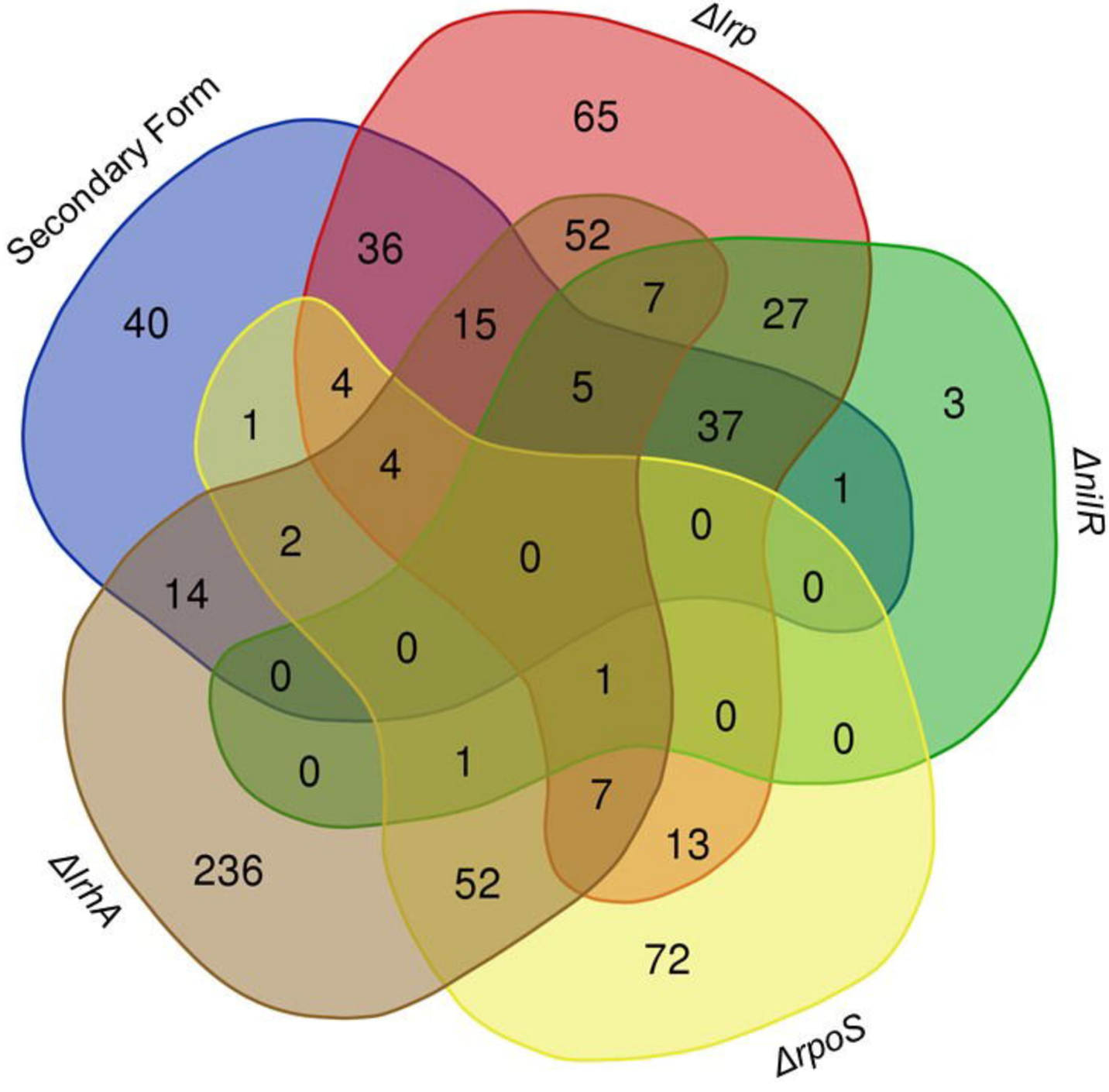

Supplementary Figure 1: Venn diagram comparing the differentially expressed transcripts between the 5 microarrays. Visualization provided from: http://bioinformatics.psb.ugent.be/webtools/Venn/

Sample Name
Sample Name
Spearman Correlation
1.00
0.75
0.50
0.25
0.00
-0.25
-0.50
-0.75
-1.00